# Distal super-enhancer drives aberrant *CXCL13* in Cancer cells driving growth and p53 dysregulation via CXCR5-CXCL13 axis

**Santosh Kumar Gothwal[1,2*], Pieta K. Mattila[3,4,5] Jacqueline H Barlow[6]**

[1] Institute of Frontier Science Initiative, Kanazawa University, Japan
[2]Central Research Resource Center, Cancer Research Institute, Kanazawa University,
[3]Institute of Biomedicine and MediCity Research Laboratories, University of Turku, Turku, Finland
[4]InFLAMES Research Flagship, University of Turku, Turku, Finland.
[5]Turku Bioscience, University of Turku and Åbo Akademi University, Turku, Finland.
[6]Department of Microbiology and Molecular Genetics, University of California, Davis, United States

* Corresponding author: skgothwal@staff.kanazawa-u.ac.jp

Key words- CXCL13, super-enhancer, CXCR5, B-lymphoma, p53, GC-migration

**Key Points**

1. Super-enhancer near *CCNG2* region interacts with *CXCL13-TSS* driving CXCL13 in cancers.
2. Aberrant CXCL13 prevents CXCR5-mediated migration of B-lymphomas and promotes growth and p53 dysregulation in CXCR5+ cells
3. CXCR5-CXCL13 axis impairs p53 target gene expression and promotes tumor growth

**Abstract**

The CXCL13 chemokine plays a crucial role in guiding B cell migration to the light zones (LZs) during the germinal center (GC) reaction. While *CXCL13* expression is absent in most cell types, aberrant amplification of the CXCR5-CXCL13 signaling is observed in various cancers, including germinal center-derived B-lymphomas (GCDBL), colorectal adenocarcinoma (COAD), and liver hepatocellular carcinoma (LIHC). However, the molecular mechanisms underlying abnormal *CXCL13* transcription in cancer cells and its functional consequences remain elusive. We identify DNA-CpG methylation binding protein 1 (MBD1) as a suppressor of *CXCL13* expression. Chromosomal conformation capture (3C) analysis reveals a distal super-enhancer located near *CCNG2* that interacts with the *CXCL13* promoter in GCDBL, suggesting that enhancer-hijacking drives the aberrant expression. Our functional validation demonstrates that CXCR5-CXCL13 signaling suppresses p53 and its target genes in GCDBLs, COAD, and LIHC. Notably, CXCL13 in the GCDBL cell line Raji disrupts CXCR5-mediated migration, a mechanism essential for (light zone) LZ-entry and affinity maturation of GC B cells. These findings highlight the dual role of the CXCR5-CXCL13 axis in immune response and cancer proliferation.

## Introduction

Chemokine (C-X-C motif) ligand 13 (CXCL13) binds and exerts signaling through the C-X-C chemokine receptor type 5 (CXCR5) and G proteins [1-4]. *CXCL13* is primarily expressed in follicular dendritic cells (FDCs), follicular helper T cells (Tfh), CD4+ T cells, CD8+ T cells, stromal cells and macrophages and regulates the innate and humoral immune repsonse [1-3, 5-9]. But aberrant *CXCL13* expression is also observed in hematological malignances such as B-cell chronic lymphocytic leukemia (B-CLL) and multiple myeloma (MM) [10-13]. Among solid cancers, *CXCL13* expression is observed in non-small cell lung carcinoma (NSCLC), breast cancers, prostate cancers and *Helicobacter pylori* associated gastric lymphomas [11, 14-18]. Aberrant CXCR5-CXCL13 signaling is evident in autoimmune diseases such as rheumatoid arthritis, [19, 20] , multiple sclerosis [21], systematic lupus erythematosis [22], primary Sjögren's syndrome [23] and myasthenia gravis [24, 25].

CXCL13 signaling is known to interfere the chemotherapeutic response and elevated CXCL13 expression by cancer cells promotes autocrine and paracrine effects in the tumor

60 microenvironment resulting [26]. CXCL13 secreted by MM cells further induces CXCL13 in
61 surrounding macrophages by Bruton's tyrosine kinase (BTK) signaling. In turn, macrophages
62 induce *CXCL13* expression in MM through TGF-β signaling [13]. Benzo(a)pyrene (BaP), a
63 carcinogen found in tobacco and air pollution, induces *CXCL13* in NSCLC [27]. *CXCL13*
64 knockdown in MM and NSCLC resulted in slower tumor growth in xenograft experiments **[13,**
65 **27]**. The CXCR5-CXCL13 axis exhibits resistance to chemotherapeutic drugs including
66 bortezomib in MM [28], and 5-flurouracil in colorectal cancer [29] and mantle cell lymphoma
67 [30]. In breast cancer, CXCR5-CXCL13 axis promotes metastasis by regulating the epithelial to
68 mesenchymal transition (EMT) [31]. CXCR5-CXCL13 signaling promotes tumorigenesis in
69 *PTEN* deficient cancers by Protein kinase C (PKC) signaling [32]. Loss of *PTEN* can induce
70 CXCL13 expression by NF-kB signaling [32]. *PTEN* is a p53 dependent gene, suggesting that
71 CXCR5-CXCL13 signaling interferes with p53 regulation, however whether the CXCR5-
72 CXCL13 axis promotes tumorigenesis by interfering with other p53 target genes is not known.
73 Despite the widespread expression of *CXCL13* in hematological and solid cancers, the
74 mechanism(s) driving aberrant *CXCL13* expression in cancer cells is elusive. Little is known about
75 the factors directly regulating the transcriptional axis of *CXCL13*. TGF-β-induced SOX4 promotes
76 the *CXCL13* expression during Th2 cells differentiation and retinoic acid and neuronal signaling
77 induces the CXCL13 expression in murine embryonic stromal cells [7, 33]. Enhancer tethering has
78 been suggested as a key mechanism for oncogene expression in cancers {Bi, 2020 #127;Dixon,
79 2012 #121;Roe, 2017 #128. Whether the CXCL13 promoter interacts with a distal enhancer that
80 drives *CXCL13* expression in cancer cells remains unknown. The chromatin insulating protein
81 CTCF links chromosome conformation and global gene-expression [34]. CTCF binding to DNA
82 is driven by local DNA methylation levels and Ten eleven translocation (TET) enzymes [35, 36].
83 DNA CpG methylation and MBD1 drive transcriptional suppression [37, 38]. Whether MBD1,
84 TET enzymes, and CTCF regulate *CXCL13* expression remains unclear.
85 In this study, we identify a super-enhancer, surrounding the *CXCL13* locus
86 interacting with *CXCL13* locus in cancer cells. Our findings in the human Burkitt's lymphoma cell
87 line Raji, suggest a role for aberrantly expressed CXCL13 in preventing migration of GCDBL
88 cells towards external CXCL13, a LZ chemokine. CXCR5-CXCL13 axis suppressed p53 target
89 genes in B-lymphomas, COAD and LIHC. These findings highlight the precise control of *CXCL13*
90 expression through epigenetic mechanisms and the regulation of enhancer-promoter interactions.

91 A loss of these regulatory processes in cancer is associated with the complex roles of CXCR5-
92 CXCL13 signaling in both hematological and solid tumors. Our study highlights the importance
93 of CXCL13 regulation in humoral immunity and tumorigenesis.
94
95 **Material and Methods**
96 **Human B lymphoma cultures and treatments**: Human B lymphoma Cell lines FL-18, FL-218,
97 FL-318, FL-518, Raji and Granta-519 were obtained from RIKEN, Japan and Kyoto university
98 hospital. All B lymphoma cell lines, THP1, LoVo and HC116 were cultured in RPMI (30264-85,
99 Nakalai) containing 10% FBS, 1% Penicillin, Streptomycin and Amphotericin B solution (Wako#
100 161-23181) in $CO_2$ incubator at 37°C under 5% $CO_2$ concentration. MCF7, HepG2 and 293T
101 cells were cultured in the DMEM containing 10% FBS, 1% Penicillin, Streptomycin and
102 Amphotericin B solution (Wako# 161-23181) in $CO_2$ incubator at 37°C under 5% $CO_2$
103 concentration. Treatment of cells with chemotherapeutics drugs Hydroxyurea (Product #085-
104 06653, Wako, Japan), Gemcitabine (product # S1714, Selleck, Japan) ATR inhibitor
105 (catalogue#KU55933; Selleck, Japan), NF-κB inhibitor (catalogue## S4902: Selleck, Japan),
106 AKT inhibitor (catalogue#S1037:Selleck, Japan) and etoposide (product #055-0843, Wako Japan),
107 bobocat339 (catalogue #SML2611, sigma), Bleomycin (Catalogue# B7116-1ML, Sigma), Nutlin-
108 3a (Catalogue# S8059, Selleck, Japan) were used as per defined timepoints and concentrations.
109 **Short hairpin knockdown, and lentivirus preparation-**
110 293T cells at nearly 60% confluency were transfected with a mix of *p-PAX2* (3 μg), *pVSVG* (3
111 μg), and target shRNA plasmids in *pLKO1-puromycin/blasticidin backbone* (3 μg). Plasmids were
112 mixed in 1 ml of Opti-Mem (Cat# 31985062, Gibco), then 27 μl of Polyethyleneimine (PEI)
113 solution (1 μg/ml) was added. After 20 minutes at room temperature, the mixture was used for
114 transfecting 293T cells. Cells were refreshed with DMEM medium after 24 hours, and culture
115 supernatants were collected 48 hours post-transfection, filtered with a 0.2 μM filter. Lentiviral
116 medium (1 ml) was used for transduction to 1 million Raji cells, followed by puromycin (1 μg/ml)
117 or Blasticidin (10 μg/ml) selection for resistance. Puromycin or Blasticidin was refreshed every
118 three days for one week. For production of CRISPR/Cas9 lentivirus, guideRNA cloned into the
119 Guide-it™ CRISPR/Cas9 Systems (Takarabio# 632601) were used instead of shRNA plasmids
120 follwed by the similar procedure and transduction to Raji cells.

121 **B Cell Migration Assay:** Transwell (Costar, REF#3421) was filled with RPMI (5% FBS) or RPMI
122 (5% FBS) medium containing rhCXCL12 (200 ng/ml) or rhCXCL13 (1000 ng/ml) (Biolegend).
123 Cell suspension of $5*10^5$ cells or $1.5*10^5$ cells for normal human B cells, isolated by institutional
124 approval and with manufacturers instruction, EasySep™ Human B Cell Isolation Kit
125 (STEMCELL technologies) were placed in transwell inserts for 6 hours at 37°C in $CO_2$ chamber.
126 Collected cells were lysed in 200 µl of CellTiter-Glo® 2.0 Reagent (Promega #G9242) and
127 allowed to stabilize for 10 minutes to measure luminescence signals. Absorbance was measured
128 using TECAN luminometer (code # MIC9414). A CXCL13-migration rescue experiment was
129 conducted in Raji cells, transfected with lentiviral particles containing CRISPR/Cas9 guide RNA
130 targeting exons 2 and 3 of *CXCL13*. Following transfection, cells were cultured for 4 days before
131 being utilized in a migration assay.
132 **FACS analysis-** Raji cells (1 * 10^6) were surface-stained with isotype controls or antibodies
133 (Supplementary Table 1) constituted in FACS buffer (PBS from Nakalai Tasque, 0.1% BSA, 0.1%
134 NaN3). After a 15-minute staining at room temperature, cells were washed, resuspended in 400 µl
135 FACS buffer, and mixed with 7-AAD before analysis. Flow cytometry was conducted using a
136 FACS Fortessa Flow cytometer (Becton Dickinson, San Jose, USA), analyzing 10,000 events with
137 data displayed as two-color plots (SSC-A/APC/PE/BV-421). Regarding CRISPR/Cas9 editing,
138 Raji cells were transfected with guide RNA targeting *CXCL13* exons 2 and 3, then sorted using a
139 ZSgreen marker.
140 **Cloning, sequence analysis and overexpression-** Full-length CXCR5 transcript amplification
141 was performed from Raji's cDNA with primers listed in supplementary Table 1. The PCR product
142 was digested with NheI and BamHI and cloned *pCMV-IRES-Puro vectors*, Sequenced and,
143 aligned with Uniprot accession (P32302). 5 µg of HpaI-linearized *pCMV-CXCR5-IRES-Puro* was
144 transfected into 1 million Raji cells via Nepagene 21 electroporation followed by Puromycin
145 selection (1 µg/ml) for a week to obtain stably transfected cells. Stable integration was confirmed
146 by PCR, flow cytometry and qPCR. The Nepagene 21 electroporation system was used according
147 to the instructions for the transient transfection of *pcDNA-MBD1*, *pcDNA-BCL6*, and *pcDNA* into
148 cell lines.
149 **RNA isolation, cDNA preparation, RT-qPCR analysis and RNA-seq datasets from GEOR-**
150 RNA from of normal Human B and B lymphoma cells was isolated (NucleoSpin® RNA kit,
151 #740984.50, Takara), cDNA was prepared (FSQ#201, Toyobo) and RT-qPCR was performed with

152 SYBR qPCR mix (QPS-201, Toyobo). The primer sequence of the analyzed transcripts is provided
153 (Supplementary table 1). Standard delta-delta Ct method was used for analysis of relative transcript
154 levels as described [39]. GSE171763 and GSE190319 datasets were used from GEO2R, NCBI.
155 Accession token (gfkvukuqnpsfvmx) and accession number GSE236240 were utilized fot the
156 cMYC and p53 ChIP-seq peaks in Raji.
157 **Immunoprecipitation and Immunoblotting–**2 million Raji cells were collected, washed with
158 PBS and lysed in 200 µl of RIPA buffer containing 1X protease inhibitors cocktail
159 (Sigma#11873580001). Lysed cells were spun at 13,000g for 10 min at 4 °C. The cell lysate from
160 supernatant was used for IP with 3 µg of CXCL13/IgG antibody (AF801, R&D system) and 20µl
161 precleared protein A beads (Invitrogen; 10001D, Invitrogen) for 2 hours at room temperatures,
162 followed by washing of the beads with RIPA buffer up to three times, 5 minutes each. The washed
163 beads were used for the elution and protein blotting. For Western blotting, cleared cell lysates
164 from 1 million cells (100 µl of RIPA) was reconstituted in 1X Lamellae buffer (Bio-Rad) with a
165 final concentration of 10% β-mercaptoethanol, followed by boiling at 95 °C for 5 min. After SDS
166 SDS-PAGE and transferring to a PVDF membrane using the Transblot® SD Semi-Dry
167 Electrophoretic Transfer Cell (Product #1703940, Bio-Rad), PVDF membranes were blocked in
168 5% skim milk for 15 min, washed with 1X TBST, and probed with primary antibody solution
169 overnight at 4 °C. The following day, the membrane was washed three times with 1X-TBST (10
170 min each) and then incubated with an HRP-conjugated secondary antibody for 1 hr. at room
171 temperature. After washing, the membrane was used to develop a chemiluminescent signal using
172 the Chemi-lumi one ultra (product #11644-40, Nakalai, Japan). The protein qualification was
173 performed using the ImageJ.
174 **Chromosome Conformation Capture (3C) Assay:** The 3C assay was performed as described
175 [39]. Two million Raji cells (-/+HU) were fixed in 1% PFA/PBS for 10 minutes, quenched with
176 glycine, and lysed in 500µl buffer (20 mM Tris-HCl, pH-8; 0.5% NP40; 1 mM EDTA, pH-8, 1X
177 protease inhibitor, Sigma #11873580001) for 30 minutes. 760 µl of 1X CutSmart buffer (NEB
178 #B6004) and 24µl of 10% SDS buffer were added, incubated at 37°C for 1 hour, followed by
179 EcoRI-digestion (40µl), overnight. The next day, 80 µl of 10% SDS was added, incubated at 65°C
180 (20 minutes), then mixed with 9.2 ml of 1X ligation-buffer, 100 µl of Triton X-100, and 1750 units
181 of Hi-T4™ DNA Ligase (NEB#M2622S). Ligation was performed at 16°C for 5 hours and
182 addition 16-18 hours at room-temperature. Samples were treated with 10 uL of RNase A (10

183 mg/ml) and 20 uL of proteinase K (20 mg/ml) before DNA purification. The DNA pellet was
184 dissolved in 600 µl TE buffer, 1µg of DNA was used for PCR (Takara, HS-Taq#R007A).
185 **Chromatin Immunoprecipitation (ChIP)-** ChIP assay was performed as described earlier [39].
186 Briefly, $2 \times 10^7$ cells were crosslinked in 50 ml of PBS with 1% formaldehyde at room temperature,
187 quenching with 2 ml of 2M glycine, followed by PBS washing, cells lysis (20mM Tris-HCL (pH-
188 8), 0.5% NP40, 1mM EDTA (pH-8), with 1X protease inhibitors, NaF (20 mM), and Na3Vo4 (1
189 µM). After brief centrifugation and nuclei collection, they were treated with SDS and 8M urea
190 buffers, followed by sonication (13 cycles, 30 sec on, 1 min off, Diagenode). Approximately 25
191 µg of chromatin was immunoprecipitated with 2 µg of antibodies, and 25 ul of Protein A/G Magna
192 ChIP beads (Sigma). The eluted samples and Input DNA were treated with RNAse and proteinase
193 K, then purified for qPCR analysis of target promoters. Primers and antibodies for qPCR are shown
194 in (supplementary table 1 and 2).
195
196 **Results**
197 **Aberrant *CXCL13* expression in hematological malignancies and solid cancers**
198 To identify cancer types exhibiting aberrant *CXCL13* expression, we explored the cancer genome
199 atlas (TCGA) sorting tumor samples by altered *CXCL13* status including deep deletion, shallow
200 deletion, diploid, gain, and amplification [40-42]. Genomic Identification of Significant Targets in
201 Cancer (GISTIC) analysis of *CXCL13* copy number alterations confirmed higher log2 copy
202 number values in gain and amplified groups compared to deep deletion, shallow deletion, and
203 diploid groups (Figure 1A). However, the levels of *CXCL13* mRNA in *CXCL13*-gain, *CXCL13*-
204 amplified, *CXCL13*-deletion and *CXCL13* shallow-deletion groups were not significantly different
205 from *CXCL13*-diploid control groups (Figure 1B). This suggests that genetic alterations such as
206 amplification and gains leading to increased copy number of *CXCL13* are not essential
207 determinants of enhanced *CXCL13* mRNA expression in cancers (Fig 1A-B) and implies that the
208 normally tight regulation of *CXCL13* expression becomes leaky in specific cancers.
209 To examine the expression of *CXCL13* mRNA among various cancers, we plotted *CXCR5*
210 and *CXCL13* mRNA Z-scores normalized with normal samples among cancer types (Figure 1C-
211 D). For both *CXCR5* and CXC13, mRNA log2 RNA-seq vs RSEM values above log2 cutoff value
212 of 1 were found in at least 1 sample for all cancers analyzed except for rectum adenocarcinoma
213 (READ) (Figure 1C,D). These results suggest that both the CXCR5 receptor and CXCL13 ligand

214 are potentially co-expressed in several cancers and may promote autocrine signaling (Figure 1C-
215 E). To evaluate whether *CXCL13* and *CXCR5* are upregulated in the same tumor, we randomly
216 identified seven CHOL samples exhibiting *CXCR5* mRNA log2 value of more than 0
217 (Supplementary Figure 1A). Four out of seven samples also exhibited *CXCL13* expression
218 (Supplementary Figure 1A), demonstrating that CHOL exhibits co-expression of *CXCR5* and
219 *CXCL13* and suggests co-upregulation may occur in multiple cancer types (Figure 1C-E,
220 supplementary Figure 1A). Downstream signaling by the CXCR5-CXCL13 axis in these cancer
221 types may promote therapy resistance (Figure 1C-E). Of note, the overall survival (OS) was
222 notably lower among high-CXCL13 expressors compared to those with lower *CXCL13* levels as
223 seen across Acute Myeloid Leukemia, Glioblastoma, and Uveal Melanoma (Supplementary Figure
224 1B-D).

225 Based on widespread *CXCL13* expression in human cancers (Figure 1A- D), we examined
226 *CXCL13* expression in human cell lines derived from hematological and solid malignancies.
227 *CXCL13* mRNA and protein expression was confirmed among Raji (Burkitt's lymphoma), Granta-
228 519 (mantle cell lymphoma), FL-518 (Follicular Lymphoma), A549, MCF7, HepG2 (LIHC),
229 HCT116, and LoVo (COADs) MDA-MB231 and THP1 cells (Figure 1F-H). These observations
230 support the notion of aberrant *CXCL13* expression in hematological and solid cancers.

231 **Induced *CXCL13* expression after chemotherapeutic treatment of cancer cells targeting DNA**
232 **replication, DNA-damage and BTK signaling**

233 Chemotherapeutic treatments in MM and NSCLC induce *CXCL13* and therapy resistance [13, 27].
234 To determine whether chemotherapeutics that induce DNA damage response and inhibit DNA
235 replication affect *CXCL13* expression in cancer cells, we investigated the effects of hydroxyurea
236 (HU), gemcitabine, etoposide, and bleomycin on *CXCL13* expression (Figure 2A-D). In Raji and
237 HCT116 cells, exposure to HU increased CXCL13 expression (Figure 2A, supplementary figure
238 2A). In contrast, γH2AX, a marker of DNA damage, was decreased in Raji cells treated with 20
239 mM HU than cells treated with 10 mM HU (Figure 2A, B). Similarly, treatment of Raji cells with
240 gemcitabine, etoposide and bleomycin increased the CXCL13 levels however no reduction in
241 γH2AX was observed upon this treatment (Figure 2A-D). Taken together, these results show that
242 DNA damage induced by various chemotherapeutics induces CXCL13 expression (Figure 2A-D).
243 It is possible that higher CXCL13 levels may counteract DNA replication stress-induced DNA

244 damage caused by HU treatment (Figure 2B). These suggest a possibility to check in future
245 whether CXCR5-CXCL13 axis promotes the γH2AX turnover and DNA-repair.
246 DNA damage and DNA replication-stress induced signaling pathways activate p53
247 [43]. Therefore, we tested if p53 activation promotes *CXCL13* expression (Figure 2D). We
248 examined the effect of Nutlin-3a treatment, an agonist of p53, on *CXCL13* levels in Raji cells
249 (Figure 2D). Nutlin-3a treatment induced the p53-dependent gene *MDM2*, but at a lower level
250 than in A549 cells which harbors a wild type p53 (Supplementary Figure 2 A, B), suggesting that
251 Nutlin-3a partially activates the mutant p53 present in Raji cells (Supplementary Figure 2A, B).
252 Intriguingly, treatment with either Nutlin-3a or bleomycin further increased *CXCL13* levels as well
253 as *CXCR5* and *CCR7*, the GPCRs expressed in GC B cells (Figure 2D, E). Surface expression of
254 CXCR5 in Raji cells was induced upon bleomycin and Nutlin-3a treatment (Figure 2E). These
255 results suggests that chemotherapeutic treatment also induce CXCR5 expression in cancer cells.
256 These results also imply a role for mutant p53 in regulation of *CXCL13, CXCR5 and CCR7*
257 expression (Figure 2D-E). In addition, treatment with Ibrutinib (a BTK inhibitor) and AZ5576 (a
258 CDK9 inhibitor) led to an upregulation of *CXCL13* expression in OCI-LY3 cells, which are an
259 activated germinal center B cell-like diffuse large B-cell lymphoma (AGC-DLBCL) cell line, as
260 well as in VAL cell line (B-lymphoma) (Figure 2F, G) [44]. This suggests that chemotherapeutics
261 agents inhibiting the BTK signaling and CDK9 inhibitors induce the *CXCL13* and CXCR5
262 expression in hematological and solid cancers. Cancer cell survival is typically promoted by
263 increased NF-kB, mTOR1C, AKT and ataxia telangiectasia and Rad3-related protein (ATR)
264 signaling [45]. To examine if these pathways affect *CXCL13* expression under DNA-replication
265 stress, we measured *CXCL13* mRNA by qRT-PCR in Raji cells treated with inhibitors against NF-
266 kB, mTOR1C, AKT, and ATR (Figure 2H) in the HU-treated Raji cells (Figure 2H). The profound
267 reduction on *CXCL13* mRNA levels was seen in response to ATR inhibition (Figure 2H). Overall
268 these suggests that chemotherapeutics agents inhibiting the DNA-replication, DNA-damage
269 response, BTK signaling and CDK9 inhibitors induce the *CXCL13* and CXCR5 expression in
270 hematological and solid cancers while ATR signaling promotes the CXCL13 signaling.
271
272 **MBD1 regulates the *CXCL13* transcription independently of CTCF**
273 By *in silico* analysis of a eukaryotic promoter database, we found putative binding sites for CTCF,
274 retinoic acid receptor alpha (RARA), p53, and MYC in the 1 kilobase upstream of the *CXCL13*

275 transcriptional start site (TSS) (Figure 3A-D). These factors also exhibited binding on the mouse
276 *CXCL13* promoter (Supplementary figure 3A-C), suggesting an evolutionary conserved regulation
277 of *CXCL13* by these factors (Figure 3A-D, Supplementary Figure 3A-C). MBD1 physically
278 interacts with RARA and promyelocytic leukemia protein (PML), leading to histone deacetylase-
279 3 mediated gene silencing [46]. Given the association among MBD1, RARA and CTCF with
280 DNA-methylation, we tested the effect of MBD1 and CTCF on *CXCL13* expression (Figure 3E-
281 F). Short hairpin (shRNA) silencing of *MBD1* and *CTCF* was confirmed in Raji cells (Figure 3F).
282 Interestingly, shMBD1-Raji cells induced *CXCL13* expression compared to scramble control
283 (shSCR-Raji) (Figure 3E), while shCTCF-Raji cells exhibited slight reduction in *CXCL13* mRNA
284 levels (Figure 3E). Compared to shMBD1 alone, shMBD1+shCTCF-Raji cells exhibited a higher
285 reduction in *CXCL13* expression (Figure 3E). These results suggest a suppressive role of MBD1
286 on *CXCL13*-expresion but a positive role of CTCF in *CXCL13* expression in MBD1-depleted
287 conditions (Figure 3E).
288 Since HU-treatment increases *CXCL13* expression in Raji and HCT116 cells (Figure 2A,
289 Supplementary Figure 2A, Figure 3E), we next examined whether MBD1 also regulates *CXCL13*
290 expression under HU treatment. Compared to HU-treated shSCR-Raji cells, HU-treated shMBD1-
291 Raji cells showed increased *CXCL13* expression (Figure 3E). The mean value of *CXCL13* mRNA
292 in HU-treated shMBD1-Raji cells was 12.3 than the mean value of 10.6 in non-HU treated
293 shMBD1 cells (Figure 3E-F). In addition, HU-treated shCTCF-Raji cells exhibited slight reduction
294 in *CXCL13* levels than the HU-treated shSCR-Raji cells (Figure 3E). Moreover, HU-treated
295 shCTCF+shMBD1-Raji cells exhibited almost equal levels of *CXCL13* expression as seen in HU-
296 treated shMBD1-Raji cells, but these levels were greater than HU-treated shCTCF-Raji cells
297 (Figure 3E). These results suggest that MBD1 plays a more important role in suppressing the
298 *CXCL13* expression under HU-treatment (Figure 3E-F). These results also suggest that CTCF
299 deficiency does not affect the upregulated levels of *CXCL13* in *MBD1*-deficient cells, suggesting
300 a downstream role of CTCF in MBD1-dependent CXCL13-regulation (Figure 3E).
301
302 Indeed, *MBD1* overexpression in Raji cells led to a stronger reduction in *CXCL13* levels in
303 response to HU treatment compared to non-HU-treated Raji cells (Figure 3F-G). Again, these
304 analyses reveal a prominent role of MBD1 in suppression of *CXCL13* expression under the HU
305 stress (Figure 3E-H). In contrast, overexpression of *BCL6*, a ubiquitously expressed protein in

306 GC B cells [47], slightly reduced CXCL13 levels in either absence or presence of HU (Figure
307 3G, Supplementary Figure 3G). The expression of *BCL6* and *MBD1* plasmids was confirmed by
308 western blotting in HEK293T cells (Supplementary Figure 3D, E).
309
310 Given that MBD1 binds to CpG-methylated DNA and promotes gene silencing [48], we next
311 aimed to clarify the role of DNA methylation in *CXCL13* expression in other B-lymphomas and
312 colon cancer cells (Figure 3H-I). From published datasets, we explored the effects of 5-
313 Azacytidine (5-Aza), on *CXCL13* expression [49, 50]. 5-Aza is a chemotherapeutic drug that
314 inhibits DNA CpG methylation [51]. Our analysis revealed that 5-Aza treatment in HT29 cells, a
315 colon cancer cell line, induced *CXCL13* expression in the 5 μM and 10 μM 5-Aza-treated groups
316 compared to the DMSO-treated groups [49] (Figure 3H, I). We also noted that 5-Aza treatment
317 increased *CXCL13* and *CXCR5* expression in OCI-LY3 cells, a DLBCL cell type [50] (Figure 3I;
318 GSE190319). These findings suggest the DNA-methylation dependent suppression of *CXCL13*
319 expression**.** Finally, to test if cMYC, which is highly amplified in Burkitt's lymphoma and the
320 Raji cells due to translocation of the MYC locus to the Immunoglobulin locus, affects CXCL13
321 levels in Raji cells, we compared the CXCL13 levels in shSCR-Raji cells to shMYC#1-Raji and
322 shMYC#2-Raji cells. The shMYC#1-Raji and shMYC#2-Raji cells showed a decrease in
323 CXCL13 expression than shSCR-Raji cells (Figure 3J), indicating a positive role of c-MYC in
324 promoting CXCL13 expression in Burkitt's lymphoma cells. These results suggest that DNA
325 methylation and MBD1 play a regulatory role in *CXCL13* expression, while cMYC positively
326 regulates CXCL13 expression.
327
328 **CTCF and RNAPII enrichment on the *CXCL13* promoter upon HU-treatment in Raji cells**
329 Since we observed a slight positive role of CTCF in *CXCL13* expression under non-HU treated
330 condition (Figure 3E), we next attempted to understand the relationship between the pattern of
331 CTCF binding on *CXCL13* promoter and its association with *CXCL13* expression. We explored
332 the CTCF ChIP-seq data from 114 cell lines available on ENCODE (Figure 4A, Supplementary
333 Figure 4A). We classified the CTCF-binding sites observed on the *CXCL13* locus in these 114
334 cell lines into three categories: site-1, site-2, and site-3 (Figure 4B). CTCF binding was observed
335 at site-1 in 47 cell lines including the normal B and prostate cells (Figure 4A). The site-1 is
336 located about 23 kb upstream of *CXCL13* TSS (Figure 4A, Supplementary Figure 4A). CTCF

337 binding at site-2, consisting of two closer consecutive CTCF peaks, was observed in 101 out of
338 114 cell lines, including the normal B and prostate cells, known to be negative for CXCL13
339 expression (Figure 4A, Supplementary Figure 4A). The consistent pattern of CTCF binding at
340 site-2 in 101 cell lines suggests a conserved binding of CTCF on the *CXCL13* locus (Figure 4A,
341 Supplementary Figure 4A). Given that most cell types do not express the *CXCL13* naturally, we
342 suggest that the conserved CTCF-binding on site-2 might be associated with suppression of
343 *CXCL13* expression (Figure 4A). In contrast, only 8 cell types exhibited CTCF binding at site-3
344 (Figure 4A, supplementary Figure 4A), which spans between exons 2 and exon 3 of the *CXCL13*
345 locus (Figure 4A, B). Interestingly, among these 8 cell types, 6 were of primary origin, while 2
346 cell lines, namely OCI-LY3 (DLBCL) and PC3 cell line (Prostate cancer), have been reported to
347 exhibit *CXCL13* expression (Figure 4A, Supplementary Figure 4A) [52]. These findings suggest
348 that CTCF binding at site-3 may be associated with an alternative conformation of the *CXCL13*
349 promoter that could facilitate *CXCL13* transcription.
350 To determine if CTCF redistribution occurs at the *CXCL13* promoter, we performed a CTCF-
351 ChIP assay in HU-treated Raji cells (Figure 4C-D). HU treatment induces *CXCL13* expression
352 (Figure 2A, 3E, Supplementary Figure 2A); therefore, altered CTCF binding at the *CXCL13*
353 promoter may be observed under HU-treated conditions. *In silico* analysis predicted dense
354 binding sites for CTCF between -1500 to -1800 and -597 and -726 on *CXCL13*-TSS (Figure 4I-
355 J); these were designated as primary pair 1 (PP1) at -1503 bp (Figure 4I-J) and primer pair 2
356 (PP2) at -754 (Figure 4C-D). CTCF binding was not detected at the PP1 site, but CTCF binding
357 was induced at the PP2 site in HU-treated Raji cells (Figure 4C-D). These suggests that HU-
358 treatment leads to CTCF-redistribution on *CXCL13* locus in Raji cells (Figure 4C-D).
359
360 Since it is unclear whether CTCF redistribution is associated with *CXCL13* expression, we
361 hypothesized that CTCF enrichment at the PP2 site might be linked to increased RNA
362 Polymerase II (RNAPII) occupancy at the *CXCL13* locus (Figure 4E). To test this, we performed
363 the RNAPII ChIP assay in HU-treated Raji cells (Figure 4E). Interestingly, we observed
364 increased RNAPII occupancy at the PP2 site (Figure 4E). Based on these findings, we propose
365 that CTCF recruitment to the *CXCL13* promoter leads to conformational changes of *CXCL13*-
366 promoter, allowing the RNAPII and transcriptional machinery to access the *CXCL13* promoter
367 and activate *CXCL13* expression under genotoxic stress.

368

369 Finally, considering the association between CTCF binding and TET2 dependent DNA-
370 demethylation [53], we investigated whether TET1/2 inhibition affect the CXCL13 expression.
371 Treatment with Bobcat-339, a potent TET1/2 inhibitor, reduced CXCL13 expression in HCT116
372 cells (Figure 4F). This suggests that TET1/2 enzymes promote CXCL13 expression in HCT116
373 cells. Although, we did not see an inhibitory effect of Bobocat-339 in Raji cells (Data not
374 shown), this suggests a cell type specific effect of Bobocat-339 on CXCL13 expression. This
375 may be possible that cell type specific genetic mutation may determine the TET1/2 activity on
376 the *CXCL13* promoter. It is noteworthy that HCT116 cells harbors wild type p53 and Raji
377 harbors two mutant p53. The p53 may interfere with TET1/2 activity on *CXCL13* promoter since
378 Nultin-3a treatment induced the *CXCL13* transcription in Raji cells (Figure 2D). Overall, these
379 results suggest a coordinated regulation among CTCF, TET enzymes, DNA methylation in
380 determining the *CXCL13* expression in cancer and normal cells.

381

382 **Distal super-enhancer of *CCNG2* locus interacts with the *CXCL13* promoter in B-lymphoma**
383 The human *CXCL13* is located on chromosome 4, and harbors 5 exons (Ensemble ID#
384 ENST00000286758; CXCL13-201; Figure 5A, Supplementary 4B). Peripheral Blood
385 Mononuclear Cells (PBMCs), including human B cells do not express *CXCL13* (Supplementary
386 Figure 5A), suggesting a closed conformation of *CXCL13* promoter in most cell types. To elucidate
387 the promoter conformation features of *CXCL13* expressing Raji cells, we assessed the binding of
388 the RNAPII subunit POL2RA along the *CXCL13* locus using ENCODE ChIP-Seq data for Raji,
389 as well as HepG2 and Ishikawa cells (Figure 5A). Strikingly, POL2RA ChIP-seq peaks were not
390 observed in near vicinity of *CXCL13* promoter in Raji, HepG2 or Ishikawa cells (Figure 5A). The
391 closest POL2RA peaks were found at -317,921 bp and -359,311 bp upstream of the *CXCL13* locus
392 (Figure 5A), while the nearest downstream peak observed in Raji, HepG2, and Ishikawa cells was
393 at +307,482 bp from the TSS (Figure 5A). Since we did not observe POL2RA peaks close to the
394 *CXCL13*-TSS, we hypothesized that a distal enhancer may drive *CXCL13* expression in Cancer
395 cells. To investigate this hypothesis, we explored the closest upstream and downstream regions
396 co-occupied with POL2RA, histone H3K4me3, and the super-enhancer specific histone marks, the
397 Histone H3K27-actyaltion (H3K27-Ac) and Histone H3K4me1 (Figure 5A). We analyzed the
398 ChIP-seq data available at the ENCODE (UCSD database; Figure 5A-B), and identified three

399 super-enhancers namely SE1, SE2 and SE3 (Figure 5A). SE1 is located between exon 2 and 3 of
400 the *CCNG2* locus, while SE2 is downstream of *CCNG2*, and SE3 was present near the *CNOT6L*
401 TSS (Figure 5A, C). The strongest POL2RA peaks were present at SE1 in Raji, HepG2 and
402 Ishikawa cells, and the POL2RA peak on SE2 was only found in Raji cells but not in HepG2 or
403 Ishikawa cells (Figure 5A). POL2RA occupancy was lower at SE2 than SE1 in Raji (Figure 5A).
404 Given that SE1 harbors the highest enrichment of POL2RA signals (Figure 5A), we hypothesized
405 that SE1 is a potential super-enhancer driving aberrant *CXCL13* expression in cancer cells. In
406 mantle cell lymphoma, as demonstrated by HiC interaction data [54], there was an observed
407 interaction between SE1 and the region flanking outside but nearer to *CXCL13* locus (Figure 5B).
408 This interaction point further exhibited another interaction with the *CXCL13* locus (Figure 5B).
409 Also, virtual circular chromosomal conformation capture (4C) from human spleen cells showed
410 the interaction between region closer to SE1 and the *CXCL13* locus (Figure 5C) [55]. These
411 suggest a possible interaction between the *CXCL13* promoter and the region near the *SE1* (Figure
412 5B,C). To test if SE1 interacts with *CXCL13* promoter, we performed chromosome conformation
413 capture assay (3C) assay using Raji cells. We checked the interaction of SE1 with predicted
414 *CXCL13*-TSS, located upstream of exon 1 [31] (Figure 5D-F). The 3C assay revealed an
415 interaction between the *CXCL13* promoter and SE1 (Figure 5D, E). To confirm the interaction
416 between SE-1 and the CXCL13 promoter, we performed the nested PCR from the purified PCR
417 products using the primer FP2 and RP2 (Figure 5E, F). The nested PCR allows amplification from
418 the first PCR containing 2069 bp product and generates a smaller band of 969 bps (Figure 5E, F).
419 The presence of smaller band of 969 bps further confirmed the SE1-*CXCL13-TSS* interaction
420 (Figure 5D-E). These results indicate that *CCNG2* super-enhancer interacts with *CXCL13*-TSS
421 and induces the *CXCL13* expression in cancer cells. Since the SE1 is enriched with RNAPII, this
422 interaction allows the access of RNAPII from SE1 to drive *CXCL13* transcription (Figure 5A,D-
423 E). Moreover, 95 cell lines from ENCODE exhibited DNase-hypersensitivity sites and a higher
424 value of GeneHancer score at SE1 (Figure 5A), suggesting the nature of open chromatin on SE1.
425 Multispecies alignment of SE1 and SE3 revealed its conservation among the other vertebrates,
426 suggesting a role for SE1 in developmentally programmed gene expression among vertebrates and
427 its leaky access in cancer cells driving he *CXCL13* expression (Figure 5F).
428

429 ***CXCL13* expression in B-lymphomas perturbs the CXCR5-migration**

430 FDCs form CXCL13 gradient in the light zone (LZ) of GCs, which attracts CXCR5-positive GC
431 B cells, and promotes their affinity maturation and selection [1, 9, 56]. Whether aberrant CXCL13
432 expression in GCDBLs serves as a programmed adaptation, promoting CXCR5-internalization and
433 deprived LZ-migration is not known. Since peripheral blood mononuclear cell including B cells
434 do no express *CXCL13* (Supplementary 5A), we hypothesized that *CXCL13* expression in
435 GCDBLs may lead to CXCR5 receptor-internalization, reducing their migration towards external
436 CXCL13. To test this, we compared CXCL13-induced migration of normal peripheral B cells
437 (NPBCs) obtained from healthy donors with GCDBLs, Raji, FL-18, FL-218, and FL-318 (Figure
438 6A-C). NPBCs efficiently migrated towards recombinant human CXCL13 (rhCXCL13), while the
439 migration index of multiple GCDBLs was significantly lower (Figure 6A). Strikingly, Raji cells
440 exhibited robust migration towards recombinant human CXCL12 (rhCXCL12), a dark zone (DZ)
441 chemokine (Figure 6B, C). This preference of Raji cells for rhCXCL12 over rhCXCL13 suggests
442 GCDBLs confinement to the DZ and hinderance to LZ entry (Figure 6B, C). To investigate if
443 internal CXCL13 disrupts CXCL13-mediated migration of GCDBLs towards an external CXCL13
444 gradient, we examined CXCL13-mediated migration of Raji cells transfected with lentivirus
445 expressing CRISPR/Cas9 guide RNA (gRNA) targeting *CXCL13* exons 2 and 3 (referred to as
446 *CXCL13*-KO Raji cells) (Figure 6D). Interestingly, bulk containing *CXCL13*-KO Raji cells
447 exhibited a significant rescue in CXCL13-migration compared to Raji cells (Figure 6D). This
448 suggests that internal CXCL13 disrupts migration of Raji cells and GCDBLs.
449 A plausible explanation of reduced migration in GCDBLs is CXCR5-internalization from
450 interaction with internal CXCL13 ligand reduces its affinity towards external CXCL13. To test
451 this, we performed co-immunoprecipitation (co-IP) of CXCL13 in Raji cells (Figure 6D). Elutes
452 of CXCL13 co-IP exhibited distinct CXCR5 signals (Figure 6D), indicating a physical interaction
453 between CXCL13 and CXCR5 in Raji cells (Figure 6D). This suggests that CXCR5-internalization
454 takes place in Raji, thus B-lymphoma cells (Figure 6D). CXCR5-internalization was also
455 confirmed by flow cytometry (FC) analysis: as intracellularly stained CXCR5 receptors were seen
456 in 100% of Raji cells while only 29% of cells were positive for surface-CXCR5 (Figure 6F-G).
457 These findings indicate internalization of surface-CXCR5 in Raji and possibly other GCDBL. Off
458 note, to confirm that *CXCR5* coding sequence mutations were not the cause of reduced CXCL13
459 migration in Raji cells, we aligned Raji *CXCR5* with human *CXCR5* (Uniprot ID# P32302),
460 revealing three SNPs (Supplementary Fig 6B). Despite these SNPs (Proline 39: CCC, Glycine 43:

461 GGT, Threonine 338: ACC), however the resulting amino acids remained unchanged, confirming
462 that Raji's CXCR5 is identical to wild type CXCR5 (Supplementary Figure 6B). Therefore,
463 alterations in the CXCR5 protein are not the cause of the altered migration of Raji cells towards
464 CXCL13. Instead, our data suggests that the internalized CXCL13 caused the impaired migration
465 of B-lymphoma cells (Supplementary Figure 6B).

466 **Accelerated cell cycle progression and suppression of p53-dependent transcripts by the**
467 **CXCR5-CXCL13 axis in hematological and solid cancers**

468 The CXCR5-CXCL13 axis activates intracellular signaling and confers chemotherapeutic
469 resistance in *PTEN*-deficient cancers [32]. Given that *PTEN* is regulated by p53, this suggests a
470 potential interference of the CXCR5-CXCL13 axis with p53 target genes. Conversely, studies have
471 shown that p53 suppresses CXCR5 [57], indicating a complex interplay between p53 and the
472 CXCR5-CXCL13 axis. Thus, the precise impact of the CXCR5-CXCL13 axis on p53 regulation
473 remains poorly understood. To investigate the effects of CXCR5 overexpression on cancer cell
474 survival, proliferation, chemotherapeutic resistance, and p53 regulation, we stably introduced the
475 *pCMV-CXCR5-IRES-EGFP* plasmid into Raji cells *(Raji-CXCR5$^{oe}$ hereafter,* Supplementary
476 figure 7A, B). Notably, *Raji-CXCR5$^{oe}$* cells displayed a marked increase in *CXCL13* levels
477 (Supplementary Figure 7C), suggesting an activation of a positive feedback loop where CXCR5
478 signaling enhances *CXCL13* expression through autocrine loop (Supplementary Figure 7A-C).
479 Despite this, *Raji-CXCR5$^{oe}$* cells did not exhibit enhanced CXCL13-migration compared to Raji
480 cells, indicating that increased CXCR5 levels did not drive CXCL13-mediated migration of
481 GCDBLs, possibly due to increased intracellular CXCL13 levels and receptor internalization
482 (Supplementary Figure 7D).

483 To assess the impact of the CXCR5-CXCL13 axis on cellular proliferation, we
484 synchronized Raji and *Raji-CXCR5$^{oe}$* cells using HU treatment. After releasing the synchronized
485 cells (Figure 7A), we monitored the live cell number (Figure 7A, B). Interestingly, *Raji-CXCR5$^{oe}$*
486 cells demonstrated significantly higher proliferation rates than Raji cells (Figure 7B). We also
487 observed elevated *JUN* levels in *Raji-CXCR5$^{oe}$* cells, a downstream target of CXCR5-CXCL13
488 signaling (Figure 7C), particularly in the presence of bleomycin or a combination of bleomycin
489 and Nutlin-3a (Fig 7C) . Compared to control Raji cells, *Raji-CXCR5$^{oe}$* cells showed increased
490 levels of *CCR7* (Figure 7C), a GPCR known to promote cancers metastasis [58]. Treatment with
491 bleomycin, Nutlin-3a, or the combination of both led to increased *CCR7* levels in both Raji and

492 *Raji-CXCR5$^{oe}$* cells (Figure 7C). However, the levels of *CCR7* were notably higher in *Raji-*
493 *CXCR5$^{oe}$* cells within their respective treatment groups compared to Raji cells (Figure 7C). In
494 contrast *Raji-CXCR5$^{oe}$* cells exhibited an overall reduction in *TP53* transcript levels compared to
495 Raji cells (Figure 7D). *TP53* transcripts were also low in individual or simultaneously treated
496 groups with bleomycin and Nutlin-3a (Figure 7D) in the *Raji-CXCR5$^{oe}$* than Raji cells , indicating
497 a potential interference of the CXCR5-CXCL13 axis in the p53 levels (Figure 7D).
498 The transcriptional targets of p53 play important roles in cell cycle regulation,
499 therefore we measured mRNA levels of *p53* target genes *CDKN1A* (encodes the p21), *DDB2*
500 (encodes a DNA-repair factor) and *PTP4A1*(encodes for a protein phosphatase required for mitotic
501 entry) between Raji and *Raji-CXCR5$^{oe}$* cells (Figure 7E). Following treatment with bleomycin,
502 Nutlin-3a, or their combination to induce p53 activation, we observed an induction of *CDKN1A*
503 and *DDB2* levels in Raji cells (Figure 7E). Interestingly, *Raji-CXCR5$^{oe}$* cells exhibited a lower
504 induction of *CDKN1A* in response to combined treatment with bleomycin and Nutlin-3a compared
505 to Raji cells treated with bleomycin and Nutlin-3a (Figure 7E). Conversely, *DDB2* levels were
506 notably higher in *Raji-CXCR5$^{oe}$* cells, particularly in the groups either treated with bleomycin or
507 co-treated with bleomycin and Nutlin-3a, compared to the corresponding treatment groups of Raji
508 cells (Figure 7E). Furthermore, the expression of *PTP4A1* was notably increased in *Raji-CXCR5$^{oe}$*
509 cells upon combined treatment with bleomycin and Nutlin-3a, as compared to its decreased
510 expression in Raji cells with similar treatment conditions (Figure 7E). This indicates that the
511 CXCR5-CXCL13 axis can impede the p53-mediated regulation of *PTP4A1, DDB2* and *CDKN1A*
512 (Figure 7D). Since Raji cells exhibited DNA-damage-induced expression of CXCL13 and CXCR5
513 (Figure 2C, D), we investigated whether this upregulation of CXCR5 and CXCL13 could enhance
514 PTP4A1 levels without the need for CXCR5 overexpression. Our observations revealed that
515 treatment of Raji cells with Bleomycin and Nutlin-3a led to nearly a twofold increase in PTP4A1
516 protein levels (Figure 7F). Moreover, this enhancement of PTP4A1 was further intensified,
517 reaching up to a fourfold increase, upon combined treatment of Raji cells with Bleomycin and
518 Nutlin-3a (Figure 7F). These findings confirm that the chemotherapeutic-induced CXCR5-
519 CXCL13 signaling can stimulate PTP4A1 expression, potentially promoting cell cycle
520 proliferation and contributing to chemotherapeutic resistance (Figure 7F). While co-treatment of
521 Raji cells with bleomycin and Nutlin-3a led to a decrease in *PTP4A1* mRNA levels, there was no
522 significant impact on protein levels. This implies that additional regulatory mechanisms may

523 regulate PTP4A1 in Raji cells following the combined treatment with bleomycin and Nutlin-3a
524 (Figure 7F).
525 Levels of p53 are regulated by ubiquitin ligases MDM2, COP1, ARF1BP1 (HUWE1)
526 and PIRH2,(Figure 7G) [59, 60]; in turn p53 can be stabilized by HAUSP-mediated de-
527 ubiquitination of p53 itself, ARF inhibition of ARFBP1 ubiquitin ligase activity, or ARF binding
528 and sequestration of MDM2 [61]. To assess how CXCR5 regulates p53, we first measured
529 expression of these ubiquitin ligases in *Raji-CXCR5$^{oe}$* cells (Figure 7G, H). Compared to Raji cells,
530 *Raji-CXCR5$^{oe}$* cells exhibited elevated levels of *PIRH2* (*RCHY1*), while no significant increase
531 was observed in *COP1* levels (Figure 7H). However, *COP1* levels were induced in Nutlin-3a-
532 treated *Raji-CXCR5$^{oe}$* cells compared to Raji cells treated with Nutlin-3a (Figure 7H). In contrast,
533 *PIRH2* levels were significantly elevated in the DMSO-treated, bleomycin-treated or the
534 combination of bleomycin and Nutlin-3a treated groups of *Raji-CXCR5$^{oe}$* cells compared to
535 respective groups in Raji cells (Figure 7H).The levels of ARF1 were decreased in *Raji-CXCR5$^{oe}$*
536 cells than Raji cells (Supplementary Figure 7E). Notably, *ARFBP1* and *MDM2* levels were also
537 reduced in *Raji-CXCR5$^{oe}$* cells than Raji cells (Supplementary Figure 7E). The levels of HAUSP,
538 which stabilizes p53 by promoting its deubiquitylation, were significantly reduced in *Raji-*
539 *CXCR5$^{oe}$* cells (Figure 7H). In contrast, *Raji-CXCR5$^{oe}$* cells treated with bleomycin, Nutlin-3a or
540 a combination of both showed a significant reduction in the *HAUSP* levels compared to respective
541 treatment grouped in Raji cells (Figure 7 H). These suggests a potential role for CXCR5-CXCL13
542 signaling in destabilizing p53 through decreased HAUSP and increased PIRH2 levels (Figure 7H).
543 These findings suggest that the CXCR5-CXCL13 axis may modulate p53 levels by disrupting the
544 balance of its ubiquitination and deubiquitinating enzymes (Figure 7H).
545 Raji cells harbor mutant p53 proteins, so we further analyzed the effect of CXCR5-
546 CXCL13 axis on p53-target genes using the HCT116 and HepG2 cells, the COAD and LIHC cell
547 lines respectively (Figure 7I, J). HCT116 and HepG2 harbor wildtype p53, which allows us to
548 examine the effect of CXCR5-CXCL13 on p53 target genes accurately. HCT116 and HepG2 cells
549 exhibit *CXCL13* expression, therefore we transiently overexpressed the *CXCR5* in HCT116 and
550 HepG2 cells to activate the CXCR5-CXCL13 axis (*HCT116-CXCR5$^{oe}$* and *HepG2-CXCR5$^{oe}$*
551 hereafter). Interestingly, *HCT116-CXCR5$^{oe}$* cells exhibited significant upregulation of *PIRH2*,
552 *MDM2*, and *PTP4A1* than HCT116 cells (Figure 7I). Furthermore, *HepG2-CXCR5$^{oe}$* cells also
553 exhibited significant upregulation of *PIRH2* and *MDM2* than HepG2 cells (Figure 7J). The most

554 induced genes were *PIRH2*, *PTP4A1*, and MDM2 in Raji, HCT116 and HepG2 after CXCR5
555 overexpression (Figure 7E-J). Collectively, these results suggest that the CXCR5-CXCL13 axis
556 promotes the expression of p53 specific ubiquitin ligases, *PIRH2* and *PTP4A1* in lymphoid and
557 solid cancers suggesting a role of CXCR5-CXCL13 axis in destabilizing the p53 levels and
558 promoting cell cycle progression (Figure 7B, H). Collectively, these results suggest that CXCR5-
559 CXCL13 axis impairs the p53 axis, promoting the tumor proliferation.
560

561 **Discussion**

562 **Regulation of *CXCL13* expression by DNA methylation, MBD1, CTCF and TET enzymes-**
563 The observed inhibitory effects of 5-Aza treatment and MBD1 on *CXCL13* expression in colorectal
564 cancer, DLBCL, and Raji cells (Figure 3E-I) are consistent with previous findings highlighting the
565 suppressive role of the DNA methylation axis on gene expression [62-64]. Furthermore, the
566 influence of TET enzymes and CTCF on *CXCL13* expression (Figures 3E, 4A-E) suggests a
567 complex interplay involving DNA methylation, MBD1, TET enzymes, and CTCF in regulating
568 *CXCL13* transcription. However, the stepwise mechanisms by which DNA methylation, MBD1
569 regulation, TET activity, and CTCF regulation affect *CXCL13* expression require further
570 investigation. We could clarify that under the DNA-replication stress, MBD1 works upstream of
571 CTCF in *CXCL13* regulation since the double knockdown of *MBD1* and *CTCF* induced the similar
572 level of *CXCL13* levels as seen in single knockdown of MBD1 (Figure 3E). On the other hand,
573 CTCF seems to also affect *CXCL13* expression under normal conditions (Figure 3E), suggesting
574 a partially non-overlapping role of CTCF and MBD1 on *CXCL13* transcription (Figure 3E). Future
575 studies should investigate whether TET enzymes affect CTCF distribution and MBD1 regulation
576 at the *CXCL13* locus in cancer cells, reported previously [53, 65, 66].

577 **ATR-signaling, TET activity and *CXCL13* expression-** We observed that DNA damage and
578 ATR signaling promote CXCL13 expression (Figure 2A, Supplementary Figure 2A, Figure 2H).
579 This suggests that DNA damage and ATR signaling may alleviate the suppressive effects of DNA
580 methylation and MBD1 on *CXCL13* transcription. This aligns with ATR's role in TET3-dependent
581 DNA demethylation and gene expression [67]. TET inhibition reduced CXCL13 expression in
582 HCT116 cells (Supplementary Figure 2A), suggesting that DNA damage and ATR signaling may
583 recruit TET enzymes to the *CXCL13* locus, leading to DNA hypomethylation and induction of
584 *CXCL13* transcription. A rational for ATR-dependent *CXCL13* transcription could be in activating

585 the autocrine signaling in CXCR5+ cancer cells, and accelerated DNA repair. This is supported
586 by observation that Raji cells treated with 20mM HU, which have higher CXCL13 levels, showed
587 lower γH2AX signals compared to those treated with 10mM HU (Figure 2A, B). This suggests a
588 novel link between ATR signaling and TET-dependent CXCL13 expression in DNA repair.

589 **CTCF, enhancer hijacking and RNAPII enrichment on the *CXCL13* promoter**

590 Using 3C assay, we identified that a distal super-enhancer (SE1) at the *CCNG2* locus interacts
591 with the *CXCL13* transcription start site (TSS) in Raji cells (Figure 5B-D). Evidence from Raji,
592 HepG2, and Ishikawa cells shows that the *CXCL13*-TSS lacks RNAPII signals at least 300 kb
593 upstream and downstream (Figure 5A). This suggests that SE1 interaction may facilitate
594 transcriptional machinery access to *CXCL13*-TSS in cancer cells (Figure 4E, Figure 5A, C). It is
595 possible that the interaction between SE1 and the *CXCL13* promoter may be regulated by TET
596 enzymes and CTCF. Supporting this, HU treatment, which induces *CXCL13* expression (Figure
597 2a, 3E) in Raji cells, leads to CTCF and RNAPII enrichment at the CXCL13 promoter (Figure 4D-
598 E). This indicates coordinated localization of CTCF and RNAPII under HU stress on *CXCL13*
599 promoter. Additionally, CTCF peaks at the *CXCL13* promoter site-3 are found in CXCL13 positive
600 OCI-LY3 and PC3 cells but not in normal B cells or hepatocytes (Figure 4A-D), suggesting CTCF
601 distribution may influence the inactive state of the *CXCL13* promoter. Further studies are needed
602 to determine whether the interaction between SE1 and the CXCL13 promoter depends on CTCF
603 redistribution, potentially altering chromosomal conformation within or beyond the associated
604 topologically associated domain, thereby facilitating RNAPII access to the *CXCL13* locus. These
605 findings align with the established interplay among TET enzymes, DNA hypomethylation, CTCF
606 binding, and chromosomal conformation changes during development [53, 65, 66].

607 **Conserved CTCF binding on *CXCL13* locus and transcriptional suppression**-The *CXCL13*
608 locus exhibits a consistent and conserved pattern of CTCF binding on site-2 in the 101 out of 114
609 examined cell lines (Figure 4A,B). Based on ENCODE ChIP-seq data sets CTCF binding at site-
610 2 of the *CXCL13* locus overlaps with RAD21 and SMC3 peaks in the normal hepatocytes. The
611 CTCF-RAD21-SMC3 may block general transcription elongation, (Nanavaty, 2020, 32333838),
612 suggesting a suppressive role of site-2 in *CXCL13* expression. It may be possible that cohesin
613 defective cells may exhibit the *CXCL13* overexpression in few cancer types. ENCODE data
614 suggest the loss of RAD21 in one sample of HepG2 in site 2, suggesting that RAD21 and
615 cohesin loss may promote the CXCL13 expression in cancer cells.

616 **Physiological elimination of B-lymphomas during humoral immune response-** CXCL13
617 expression in B-lymphomas may represent a programmed adaptation that restricts their migration
618 to the LZ by CXCR5-internalization and confines them to the DZ. This restriction could potentially
619 limit survival feedback signaling from FDCs, leading to the GCDBLs elimination. The
620 orchestrated *CXCL13* expression via CTCF and altered chromosome conformation (Figure 3A-D,
621 Figure 5A-D) might hinder the LZ-migration and fate of GC B cells. Moreover, Burkitt's
622 lymphomas, and myeloma exhibit translocations between the immunoglobulin heavy and *MYC*
623 loci [68-70], resulting in MYC overexpression. MYC is required for LZ entry of GC B cells [71].
624 The amplified *MYC*, leading to CXCL13 overexpression, may simultaneously prevent the LZ entry
625 of GCDBLs, suggesting a dual role for MYC in regulating the fate of germinal center B cells. This
626 indicates a unique adaptation within GCDBLs, where MYC and oncogenic factors like BCL6 may
627 paradoxically serve tumor-suppressive roles by preventing the exit of GCDBLs from GCs [72].
628 These regulations assist the robust immune response by facilitating the elimination of GCDBLs
629 and promoting the generation of high-affinity antibodies. Furthermore, internalized CXCR5 may
630 undergo proteasomal degradation in GCDBLs and needs to be tested in future studies.
631 **Chemotherapeutic resistance -** The inducibility of CXCL13 and CXCR5 by DNA damage-
632 inducing chemotherapeutics highlights potential concerns on resistance caused by CXCR5-
633 CXCL13 axis in cancer cells (Figure 2A-D, Supplementary Figure 2A). We show that the CXCR5-
634 CXCL13 axis can counteract p53 levels by increasing expression of the ubiquitin ligase *PIRH2*
635 and reducing the expressions of its de-ubiquitylation enzyme, *HAUSP* (Figure 7H-I). CXCR5-
636 CXCL13 signaling also counteracted the p53 target genes *PTP4A1*, *DDB2* and *CCR7* (Figure 7D-
637 I), which could potentially promote cell cycle progression, DNA repair and metastasis. It will be
638 important to see if *PTP4A1*/*CCR7/DDB2* knockdown in CXCR5 and CXCL13 co-expressing
639 cancers perturbs tumor growth in xenograft models. *PTP4A1* and *CCR7* could be novel markers
640 exhibiting chemotherapeutic-resistance in the cancer exhibiting the CXCR5-CXCL13 signaling.
641

642 **Declarations**

643 **Ethical Approval** – The use of human B cells/ cell lines was approved as per Institutional ethical
644 board.

645 **Competing interests-** The authors declare no competing interest financially.

**Authors' contributions-** SKG designed the original hypothesis, performed experiments, and analyzed data. PM discussed the results and provided constructive feedback. SKG wrote the manuscript. JHB critically read the manuscript and provided constructive feedback. All authors read and agreed to manuscript.

**Funding-** This work is supported grant number 21K16142 from Japan Science for promotion sciences (JSPS) to SKG .

**Availability of data and materials-** All data needed to evaluate the conclusions in the paper are present in the main text and the supplementary materials.

**Acknowledgment-** The authors acknowledge TCGA and the ENCODE Consortium for generating data used in this study. We thank Dr. Katsuya Sakai for anti-goat IgG-HRP antibody. We thank Dr Susumu Kohno for gifting shMYC plasmids. We thank Dr. Atsuyasu Sato for the discussion. We thank Dr. Atsushi Hirao for providing the THP1 cells and Dr. Kazuhiro Murakami for useful discussions and providing the HCT116 and LoVo cell lines, we thank Dr. Y. Endo for HepG2 cells. We thank Dr. Takeshi Suzuki for the supporting SKG's research at Kanazawa University.

**Limitations of the study: Limitations of the study:** In this study, we have identified and characterized a potential mechanism that inhibits *CXCL13* expression in adherent cells, as CXCL13 is typically expressed in certain immune cells. Our findings suggest that the suppression of *CXCL13* expression involves DNA methylation factors and a redistribution of CTCF on the *CXCL13* promoter, leading to a conformational change that transitions the promoter to a transcriptionally active state. However, further investigation is required to elucidate whether DNA methylation and TET activity coordinate these changes, and how the loss of DNA methylation and CTCF redistribution influences this altered chromosomal conformation and RNAPII enrichment on *CXCL13* promoter to activate transcription. Additionally, the CTCF boundaries that overlap with RAD21 and SMC3 seem to play a regulatory role in the polyadenylation of *CXCL13* mRNA, potentially resulting in various *CXCL13* transcript forms. Therefore, transcriptional elongation may be perturbed by the RAD21/CTCF/SMC3 sites on intron 2, producing alternatively spliced *CXCL13* transcripts. We have not addressed the alternative splicing of *CXCL13* in this manuscript. Our study does not conclusively distinguish the forms of the CXCL13 protein reported. This is also to note that the CXCL13 molecular weight appears higher than the predicted 13 kDa band. This will also help clarify whether intracellular CXCL13 expression contributes to CXCR5

677 receptor internalization. Attempts to generate viable CXCL13-knockout cell lines other than in
678 Raji cells may be necessary to resolve this concern. A secretory form of CXCL13 may arise from
679 the reported variant, which could impact on CXCR5-CXCL13 signaling in autocrine and paracrine
680 mode, but its appearance may not be visible on WB due to secretion. These limitations warrant
681 further investigation in future studies.
682
683 **Figure legends-**
684 **Figure 1 *CXCL13* is expressed in hematological, and solid cancers** (A) *CXCL13* putative copy
685 number values from GISTIC vs log2 copy number values in 10712 samples. p values <0.0001 are
686 derived from ordinary one-way ANOVA (B) *CXCL13*: mRNA expression z-scores relative to
687 normal samples (log RNA-Seq V2 RSEM) data are from 6909 samples in both axes. *ns* = not
688 significant; p value derived from ordinary one-way ANOVA (C) *CXCR5*: mRNA expression z-
689 scores relative to normal samples (log2 RNA Seq V2 RSEM from 6959 diploid samples *RSEM=*
690 *RNA-seq* by expectation-maximization. X axis profile shows TCGA cancer acronyms. Dotted line
691 in parallel to X axis separates the tumor samples exhibiting cutoff *CXCR5 mRNA* log2 values >1
692 or log2<1. TCGA Cancer acronyms: rectum adenocarcinoma (READ), bladder urothelial
693 Carcinoma (BLCA), breast cancer (BRCA), cholangiocarcinoma (CHOL), colon adenocarcinoma
694 (COAD), esophageal carcinoma (ESCA), head and neck squamous cell carcinoma (HNSC),
695 kidney chromophobe (KICH), Kidney renal clear cell carcinoma (KIRC), kidney renal papillary
696 cell carcinoma (KIRP), liver hepatocellular carcinomas (LIHC), lung adenocarcinoma (LUAD),
697 lung squamous cell carcinoma (LUSC), prostate adenocarcinoma (PRAD), stomach
698 adenocarcinoma (STAD), thyroid carcinoma (THCA), uterine corpus endometrial carcinoma
699 (UCEC) (D) *CXCL13*: mRNA expression z-scores relative to normal samples (log RNA Seq V2
700 RSEM) in 6953 diploid samples. X axis shows TCGA cancer acronyms. Dotted line in parallel to
701 X axis separates the tumor samples exhibiting cutoff *CXCL13 mRNA* log2 values >1 or log2<1 (E)
702 Schematic of CXCR5 and CXCL13 overexpressing cancer cells in activating autocrine, paracrine
703 signaling, and metastasis to distally located CXCL13 chemokine gradient. (F) Ethidium bromide
704 gel-electrophoresis of *CXCL13* PCR using the cDNA samples from normal human peripheral B
705 cells, Raji and Granta-519 cells (G) Relative quantitative real-time PCR (qRT-PCR) analysis
706 comparing the mRNA levels of *CXCL13* versus *ACTB* in Raji, FL-518, Granta-519, A549, and
707 MCF7 cells. Additionally, quantification of *CXCL13*, *CXCR5*, and *CCR7* mRNA levels in multiple
708 human B cell lymphoma cell lines (Raji, FL-518, Granta-519), along with breast cancer (MCF7)
709 and lung cancer (A549) cell lines. *CXCL13* mRNA levels in the other cell lines are normalized to
710 those in A549 cells. Turkey's multiple comparison test for statistical significance. *p= 0.0486* for
711 Raji cells vs A549 cells and *p= 0.0430* for Raji cells vs MCF-7 cells. Data are mean ± SEM for
712 n=3 (H) CXCL13 Western blotting using LoVo (COAD), HCT116 (COAD), HepG2 (LIHC),
713 MDAMB-231 (BRCA) and THP1 (Acute monocytic leukemia) cell lysates.
714

715 **Figure 2- DNA damage and Replication stress induce *CXCL13* expression in the Raji cells-**
716 (A) Western blotting of CXCL13 and γH2AX from the cell lysates of Raji cells treated with
717 DMSO, hydroxyurea (10 mM and 20 mM), Gemcitabine (20μM and 40μM) and Etoposide
718 (50μM and 100μM) for 24 hours. Values above blot indicate densitometric qualification of
719 CXCL13 normalized to β-actin levels from a representative blot (B) Correlation of densitometry
720 quantification of CXCL13 and γH2AX signals in Raji cells treated with HU, Gemcitabine and
721 Etoposide, normalized with CXCL13/γH2AX levels of DMSO treated Raji cells (C) CXCL13
722 expression analysis by Western blotting in Raji cells treated with Bleomycin (5μg/ml) for 24 hrs.
723 Values above blot indicate densitometric qualification of CXCL13 normalized to β-actin levels
724 from a representative blot (D) qRT-PCR analysis of *CXCL13*, *CXCR5*, *TP53* and CCR7 mRNA
725 levels in Bleomycin (5μg/ml) treated Raji cells, Nutlin-3a (10μM) treated Raji cells and
726 Bleomycin (5μg/ml) + Nutlin-3a (10μM) treated Raji cells are shown. ***CXCL13***: p= 0.0409 in
727 Raji (DMSO vs Bleomycin), p= 0.5163 (DMSO vs Nutlin-3a), p= 0.0002 [bleomycin vs
728 (Nutlin-3a+Bleomycin)], p <0.0001 for [Nutlin-3a vs (Nutlin-3a+Bleomycin)]. Šídák's multiple
729 comparisons test. ***CXCR5***; p <0.0001 [DMSO vs (Nutlin-3a+Bleomycin)]. ***CCR7***; p <0.0001
730 [DMSO vs (Nutlin-3a+Bleomycin)]. Dunnett's multiple comparisons test. Data are presented as
731 mean ± SEM; n=3; p<0.0001 for DMSO versus Bleomycin treated groups, p<0.0001 for DMSO
732 versus Nutlin-3a (10μM), and p<0.0001 for DMSO vs co-treatment with Bleomycin (5μg/ml)
733 and Nutlin-3a (10μM). (E) Surface expression of CXCR5 in Raji cells in Raji cells treated with
734 Bleomycin (5μg/ml), Nutlin-3a (10μM), and the combination of Bleomycin (5μg/ml) + Nutlin-3a
735 (10μM). (F) Treatment with Bruton Tyrosine Kinase Inhibitor Ibrutinib to OCI-LY3 for 48 hrs
736 induced *CXCL13* transcripts per million reads (TPM). Unpaired t-test, *p = 0.0004* (G) Panel of
737 OCI-LY3 and VAL cell lines treated with AZ-5576, a selective CDK9 inhibitor, exhibiting
738 induced *CXCL13* TPM (GSE113035) in at least 1/2 independent samples. (H) effect of 24 hr
739 treatment of NF-κB inhibitor (10mM), AKT inhibitor (10μM), ATR inhibitors (10μM),
740 mTOR1C (10μM) treatment on *CXCL13* mRNA expression in the Raji cells. Data are mean ±
741 SEM of three independent experiments. Ordinary one-way ANOVA. *p*= 0.0118 for *HU vs HU +*
742 *ATRi* groups.
743
744 **Figure 3- MBD1 suppresses the *CXCL13* expression independently of CTCF** (A) *In silico*
745 binding of RARA, MYC, p53 and CTCF on *CXCL13* promoter predicted by eukaryotic promoter
746 database. Factors binding to promoter with a cutoff p value > 0.001 are shown. Binding sites of
747 RARA at -242, -824, -941, -961 from the *CXCL13*-TSS (B) Binding sites of CTCF at -67, -597, -
748 726 from TSS (C) Binding sites for p53 at -633, and -634 from TSS (D) Binding sites for MYC
749 at -410, -716 and -717 from TSS (E) qRT-PCR quantification of *CXCL13* mRNA in -/+ HU
750 treated shSCR-Raji, shMBD1-Raji, shCTCF-Raji and (shMBD1+shCTCF)-Raji cells. Data are
751 mean ± SEM for three independent replicates. *p* values are derived from ordinary one-way
752 ANOVA (*p<0.0001=****)* (F) qRT-PCR analysis of the *MBD1* and *CTCF* in shSCR-Raji,
753 shMBD1-Raji, shCTCF-Raji and (shMBD1+shCTCF)-Raji cells. Data are mean ± SEM for three
754 intendent replicates. *p* values are derived after Šídák multiple comparison test (G) CXCL13

755 Western blotting using Raji cell lysates transfected with *pcDNA-3.1*, *pcDNA-MBD1* and *pcDNA-*
756 *BCL6* for 24 hours followed by 10 mM HU treatment for 24 hours. Cell lysates were prepared
757 48 hrs post-transfection and 24 hr. post HU treatment and then subjected to *CXCL13* western
758 blotting. Values above blot indicate densitometric qualification of CXCL13 normalized to beta-
759 actin levels from a representative blot (H) HT29-cells treated with 5-Aza induces the *CXCL13*
760 expression. HT-29 cells treated with dimethyl sulfoxide (vehicle alone= 0 μM 5-Aza), 5μM 5-
761 Aza and 10 μM 5-Aza for five days. Normalized transcripts per million (TPM) values of the
762 *CXCL13* is shown. Two treated sample out of three samples exhibited the upregulation of
763 *CXCL13* transcript (I) 5-Azacytidine treatment of OCI-LY3 cells induced *CXCL13* and *CXCR5*
764 transcript levels (GSE190319). Normalized TPM values are shown in the graph (J) WB of
765 CXCL13 using the cell lysates from shSCR-Raji, shMYC#1-Raji, shMYC#2-Raji cells lysates.
766 Data are representative of three independent repeats.
767
768 **Figure 4- Enrichment of CTCF and RNAPII on *CXCL13* promoter in HU-treated Raji cells**
769 (A) CTCF-ChIP-seq and distribution of CTCF binding on site-1, site-2 and site-3 on CXCL13
770 locus in normal human B cells, prostate cells and the OCI-LY3 and PC3 cell lines. The
771 additional peak of CTCF on site-3 is located at position, chr4:77606576-77606790. Peak 1
772 sequence Position: chr4:77578302-77578777. Position of peak 2 from: chr4:77599430-77599754
773 OCI-LY3 and PC3 cell lines exhibit the *CXCL13* expression (B) Distribution of CTCF's
774 presence/absence on site-1, site-2 and site-3 in 114 cell types. Data represent the percentage of
775 either presence or absence of CTCF peaks on site-1, site2 and sire-3 among 114 cell lines tested
776 for CTCF ChIP-seq peaks. Loss of CTCF binding on either 1 or both peaks on Site-2 is counted
777 as absence of CTCF binding. Data are derived from transcription factor ChIP-seq peaks from
778 129 cell lines on ENCODE from the UCSD genome browser (C) Schematic of CTCF putative
779 binding sites on *CXCL13* locus at PP1 and PP2 sites located at -1503 and -597 upstream of the
780 TSS respectively (D) CTCF ChIP-signals (%) on PP2 site in -/+HU treated Raji cells. Data are
781 mean ± SEM for n=3. p= 0.0284 (unpaired t test) (E) RNAPII ChIP-signals (%) on PP2 site in -
782 /+HU treated Raji cells. Data are mean ± SEM for n=3 p= 0.0058 (unpaired t test) (unpaired t
783 test) (F) HCT116 cells were treated with DMSO and 10μM, 20μM, 40μM and 80μM
784 concentrations of Bobocat-339 for 24 hours. After the treatment period, the cells were lysed, and
785 proteins extracts were tested to assess the expression levels of CXCL13 by western blotting
786 analysis.
787
788 **Figure 5- Distal super enhancer at *CCNG2* locus interacts with *CXCL13* promoter (A)**
789 (A) Genetic features of the *CXCL13* locus are depicted using the UCSD Genome Browser with
790 Three super-enhancers surrounding the *CXCL13* locus, namely SE1, SE2, and SE3 are shown in
791 maroon. Histone marks H3K4me3, H3K27Ac, and H3K4me1 are displayed from seven cell lines
792 from the UCSD database. Super-enhancers highlighted in maroon and their overlapping with
793 H3K27Ac and H3K4me1 signals. POL2RA ChIP-seq signals from ENCODE3 near the *CXCL13*
794 locus are shown for Raji, HepG2, and Ishikawa cells. Comparison maps of micro-C and Hi-C

795 interactions, GeneHancer regulatory elements, and DNase clusters of the *CXCL13* locus are
796 presented from the UCSD database (B) HiC interaction data: Mantle cell lymphoma (left) and
797 normal GC B cells (right). In the mantle cell lymphoma HiC map, the highlighted rectangle
798 indicates an interaction between the *CCGN2* region and an area outside the *CXCL13* promoter,
799 which also interacts with *CXCL13* promoter (C) Virtual Circular chromosomal conformation
800 capture (4C) from spleen exhibiting the genomic interaction of *CXCL13* locus. Assembly hg19,
801 resolution 40,000 base pairs (D) Schematic representation of the super-enhancer identification
802 and their possible interaction with the *CXCL13* transcription start site (TSS). SE1, SE2, and SE3
803 exhibit overlapping signals of POL2RA, H3K27Ac, and H3K4me1. Schematic of SE1, SE2 and
804 SE3 interaction with the super-enhancer located at *CCNG2* or *CNOT6L* (E) Schematic
805 representation of 3C assay with EcoR1 digestion. Primer locations are shown for the detection of
806 the first PCR and nested PCR products using primer pairs (FP1+RP1) and (FP2+RP2),
807 respectively. The band lengths of the first PCR and nested PCR are 2069 and 1100 bp,
808 respectively (F) Ethidium bromide staining of 3C assay PCR products. PCR performed with
809 1000 ng of purified genomic DNA from control Raji or 3C-processed (-/+HU) Raji cells. The
810 nested PCR product for positive interaction between SE1 and *CXCL13*-TSS is shown with arrow
811 in right (G) UCSD genome browser-based conservation of SE1, SE3 among 100 vertebrates by
812 PhastCons and Multiz alignment is shown.
813
814 **Figure 6- CXCL13 expression is human GCDBLs perturbs migration due to CXCR5-**
815 **internalization (A)** Migration index of normal Human B and multiple Human B lymphoma lines
816 Raji, FL-18, FL-518 and Granta-519 cell migration towards rhCXCL13 gradient. Data are mean
817 ± SEM. P values for migration index were calculated using ordinary one-way Anova with
818 multiple comparison. $p$= 0.002 for normal human B vs. FL-18, $p$<0.0001 for normal Human B
819 vs FL-218, normal human B vs FL-318 and normal Human B vs Raji cells (B) Raji cells migrate
820 efficiently towards rhCXCL12 (200 ng/ml). Data are mean ± SEM for n=3. NC= Negative
821 control exhibiting the cell migrated to empty medium without the rhCXCL12 gradient (C) Raji
822 cells exhibit enhanced migration towards rhCXCL12 compared to rhCXCL13 (n=3). The
823 migration index of Raji cells towards rhCXCL12 was significantly higher than towards
824 rhCXCL13 (p = 0.0006, unpaired Student's t test) (D) Comparison of migration index between
825 Raji cells and *CXCL13*-KO Raji cells towards rhCXCL13. *CXCL13*-KO Raji cells exhibit
826 increased migration towards rhCXCL13 compared to control Raji cells (Data presented as mean
827 ± SEM for n=3, p values calculated using unpaired t test) (E) Co-immunoprecipitation of
828 CXCL13 and CXCR5 in Raji cells. Immunoprecipitation was performed using 100 µg of protein
829 lysates from Raji cells with CXCL13 antibody (ab) or IgG antibody, followed by elution and
830 Western blotting for CXCL13 and CXCR5 (F) Intracellular CXCR5 in Raji cells was detected
831 using a CXCR5 antibody, followed by probing with a PE-conjugated secondary antibody.
832 Unstained and isotype controls were used for flow cytometry staining. (G) Surface CXCR5
833 staining in Raji cells was performed with an APC-labelled CXCR5 antibody.
834

**Figure 7. CXCR5 Modulates Cell Cycle Progression and Overrides p53 response**
(A) Schematic representation of cell synchronization by HU-treatment of Raji and *Raji-CXCR5*$^{oe}$ cells (B) Enhanced proliferation in *Raji-CXCR5*$^{oe}$ cells compared to Raji cells. Cell proliferation assessed on days 0, 2, 4, and 6 with data from four replicates, plotted as multiples of ($1*10^5$) cells on the X-axis (C) Treatment of Raji and *Raji-CXCR5*$^{oe}$ cells with Bleomycin (5µg/ml), Nutlin-3a (10µM), or their combination for 24 hours and qRT-PCR quantification of *JUN* and *CCR7* transcript levels in *Raji-CXCR5*$^{oe}$ cells compared to Raji cells. *JUN* transcript is shown as downstream positive marker gene induced from CXCR5-CXCL13 signaling. p= 0.0002 for Raji (Bleomycin) vs *Raji-CXCR5*$^{oe}$ (Bleomycin): p= 0.0336 for Raji (Nutlin-3a) vs *Raji-CXCR5*$^{oe}$ (Nutlin-3a): p= 0.0002 in Raji (Nutlin-3a+bleomycin) vs *Raji-CXCR5*$^{oe}$ (Nutlin 3a+bleomycin) groups. Šídák's multiple comparisons test. For *CCR7* transcripts; p= 0.0022 for for Raji (DMSO) vs *Raji-CXCR5*$^{oe}$(DMSO) and p<0.001 for Raji vs *Raji-CXCR5*$^{oe}$ in all three respective treatment groups. Šídák's multiple comparisons test. Data presented as mean ± SEM for n=3. (D) qRT-PCR quantification of *TP53* transcript levels in *Raji-CXCR5*$^{oe}$ cells compared to Raji cells. p =0.0025 in Raji (DMSO) vs *Raji-CXCR5*$^{oe}$(DMSO) , p=0.0064 Raji (bleomycin) vs *Raji-CXCR5*$^{oe}$(Bleomycin) , p= 0.0114 for Raji (Nutlin-3a) vs *Raji-CXCR5*$^{oe}$(Nutlin-3a) and p= 0.0052 for Raji (bleomycin+Nutlin-3a) vs *Raji-CXCR5*$^{oe}$(Bleomycin+Nutlin-3a) cells. p values are derivatives of t test. Data presented as mean ± SEM for n=3 (E) Treatment of Raji/*Raji-CXCR5*$^{oe}$ cells with Bleomycin (5µg/ml), Nutlin-3a (10µM), or their combination and mRNA quantification of p53 target genes, *CDKN1A*, *DDB2* and *PTP4A1*. p <0.0001 for *CDKN1A*, *DDB2*, *PTP4A1* in Raji (Bleomycin+Nutlin-3a) vs *Raji-CXCR5*$^{oe}$(Bleomycin +Nutlin-3a). p values are derived with Tukey's multiple comparison test. Data presented as mean ± SEM for n=3 (F) Treatment of Raji cells with Bleomycin (5µg/ml), Nutlin-3a (10µM) for 24 hr and Western blotting analysis of PTP4A1 and γH2AX using whole cell lysates. PTP4A1 levels were increased after bleomycin and Nutlin-3a treatment of Raji cells. Values above blot indicate densitometric qualification of PTP4A1 normalized to β-actin levels. Data are representative of three independent replicates (G) Schematic representation of enzymes regulating the ubiquitination/de-ubiquitylation of p53 (H) Treatment of Raji/*Raji-CXCR5*$^{oe}$ cells with Bleomycin (5µg/ml), Nutlin-3a (10µM), or their combination and qRT-PCR quantification of *COP1*, *PIRH2* and *HAUSP* in *Raji-CXCR5*$^{oe}$ cells compared to Raji cells. p< <0.0001 for *COP1* in Raji (Nutlin-3a) vs *Raji-CXCR5*$^{oe}$ (Nutlin-3a). p= 0. 0.0118 for *PIRH2* in Raji (DMSO) vs *Raji-CXCR5*$^{oe}$(DMSO) , p<0.0001for *PIRH2* in Raji (Bleomycin) vs *Raji-CXCR5*$^{oe}$(Bleomycin). p <0.0001 for *HAUSP* in all respective treatment groups of Raji vs *Raji-CXCR5*$^{oe}$ cells. Tukey's multiple comparisons test. Data presented as mean ± SEM for n=3 (I) HCT116 and *HCT116-CXCR5*$^{oe}$ cells utilized for qRT-PCR analysis for *DDB2*, *MDM2*, *PIRH2*, and *PTP4A1* mRNA levels. p= 0.276680 (*DDB2*), p= 0.000845 (*PIRH2*), p= 0.001291 (PTP4A1), p= 0.000005 (MDM2) in HCT116 vs *HCT116-CXCR5*$^{oe}$ cells. Unpaired t test. Data presented as mean ± SEM for n=3. (J) HepG2 and *HepG2-CXCR5*$^{oe}$ cells utilized for qRT-PCR analysis of for *DDB2*, *MDM2*, *PIRH2*, and *PTP4A1* mRNA levels. p= 0.126974 (*DDB2*), p= 0.00017 (*PIRH2*), p=

874 0.026746 (PTP4A1), p= 0.000404 (MDM2) in HepG2 vs *HepG2-CXCR5$^{oe}$* cells. Unpaired t test.
875 Data presented as mean ± SEM for n=3.
876
877 **Supplementary Figure 1** (A) Comparison of *CXCR5* and *CXCL13* expression in 7 CHOL
878 samples revealed co-expression of both *CXCR5* and *CXCL13* in 4 samples. Co-expression
879 indicates a possible autocrine signaling in these cancers. (B-D) Overall survival analysis from
880 *GEPIA* (Gene Expression Profiling Interactive Analysis) indicates that groups with low *CXCL13*
881 TPM and high *CXCL13* TPM for Uveal Melanoma (UVM), Glioblastoma (GBM), and Acute
882 Myeloid Leukemia (AML) demonstrate varying survival outcomes. The *CXCL13*-high TPM
883 groups exhibit reduced survival rates in these cancer types (E) Detection of CXCL13 in cell
884 lysates of Raji cells, CRISPR/Cas9 transfected Raji cells with guide RNA targeting
885 *MYC*/*CXCL13* cells. The THP1 cell line serves as a positive control, expressing CXCL13.
886 Antibody:Novus#AF801. Cell lysates of CRISPR/Cas9 transfected Raji cells were prepared after
887 transfection with CRISPR/Cas9 plasmid targeting exon 2 and 3 of *CXCL13* locus, followed by
888 culture for 2-days prior to sorting of transfected cells. Sorted cells were subsequently cultured
889 and single cell clones were grown until confluency and viability. The single-cell clones
890 (*CXCL13$^{-/+}$*) were then subjected to Western blot analysis. The SDS-PAGE gel concentration
891 used was 12%, and the transfer was conducted for 20 minutes. Homozygous clones *(CXCL13$^{-/-}$)*
892 of Raji cells could not grow faster and maintained in passage. The Western blot was conducted
893 using a bulk of sorted cells that were positively transfected with CRISPR/Cas9, following their
894 culture until viability was maintained. CXCL13 appeared around 22 kilodaltons (kDa), which
895 aligns with the weight of CXCL13 in THP1 cells—a positive control cell line expressing
896 CXCL13 and is reduced in two independent *CXCL13$^{+/-}$* clones of Raji cells.
897
898
899 **Supplementary Figure 2**
900 (A) Western blotting of CXCL13 and γH2AX from the cell lysates of HCT116 cells treated with
901 DMSO, hydroxyurea (10 mM and 20 mM), Gemcitabine (20μM and 40μM) and Etoposide
902 (50μM and 100μM) for 24 hours (B) Western blotting analysis of MDM2, p53, γH2AX and β-
903 actin in Raji cells treated with Bleomycin (5μg/ml), Nutlin-3a (10μM), or the combination of
904 Bleomycin (5μg/ml) + Nutlin-3a (10μM). (C) *MDM2* mRNA levels in the Raji/A549 cells
905 treated with Nutlin-3a (10μM) for 24 hrs. Data are presented as mean ± SEM for n=3 samples.
906
907 **Supplementary Figure 3**
908 CTCF, RARA, Myc, and p53 binding sites are evolutionarily conserved on the *CXCL13*
909 promoter (A) RARA binding sites are located at -216, -336, -399, and -796 from the
910 Transcription Start Site (TSS) (B) Predicted CTCF binding sites are at 74, 34, -131, and -749
911 from the TSS (C) Predicted Myc binding site is at -622 from the *CXCL13*-TSS. (D) Western
912 blotting of MBD1 in *pcDNA-MBD1* (1 μg) overexpressing H3K293T cells post 24 hr of

913 transfection (E)Western blotting of BCL6 in *pcDNA-BCL6* (1 µg) overexpressing HEK293T
914 cells post 24 hours of transfection.
915
916 **Supplementary Figure 4**
917 (A) CTCF-ChIP-seq and distribution of CTCF binding on site-1, site-2 and site-3 on CXCL13
918 locus in 114 cell lines including of normal human B cells and OCI-LY3. The additional peak of
919 CTCF on site-3 is located at position, chr4:77606576-77606790. Peak 1 sequence Position:
920 chr4:77578302-77578777. Position of peak 2 from: chr4:77599430-77599754 (B) Genomic
921 Locus of human *CXCL13*. Ensemble Genome Browser view of the CXCL13 exon-intron
922 position (transcript ID# ENST00000286758.4 CXCL13-201).
923
924 **Supplementary Figure 5**
925 (A) Expression status of genes neighboring the *CXCL13* locus—SEP11, CCNI, CCNG2,
926 CNOT6L, and MRPL1—in peripheral blood mononuclear B cells (PBMCs) is displayed, as
927 assessed from PBMC data (Hao et al., 2020).
928
929 **Supplementary Figure 6**
930 Sequencing of CXCR5 coding region in Raji cells (A) Absolute similarity in the peptide sequences
931 derived from *CXCR5* DNA clones of Raji cells with human *CXCR5*. Uniport alignment of the
932 CXCR5 protein from Raji cells and the human CXCR5 peptide from Uniprot. Three single
933 nucleotide polymorphisms (SNPs) in Raji's CXCR5 (Proline 39: CCC, Glycine 43: GGT,
934 Threonine 338: ACC) did not resulted in amino acids confirming the reduced migration of Raji
935 towards CXCL13 is not caused by *CXCR5* mutations.
936
937 **Supplementary Figure 7**
938 CXCR5 Overexpression induces *CXCL13* mRNA expression via positive feedback in Raji cells
939 (A) Flow cytometry analysis of CXCR5 surface staining reveals elevated CXCR5 levels in *Raji-*
940 *CXCR5$^{oe}$* cells compared to normal Raji cells (B, C) Quantification of *CXCR5* and *CXCL13*
941 transcripts using qRT-PCR in *Raji-CXCR5$^{oe}$* cells compared to Raji cells. The data represent
942 mean ± SEM for n=3, with p-values < 0.0001 and < 0.0306, respectively (D) Migration assays
943 against rhCXCL13 gradient in Raji and *Raji-CXCR5$^{oe}$* cells. Data presented as mean ± SEM for
944 n=3 (E) qRT-PCR analysis of the expression levels of *ARF1*, *ARFBP1*, and *MDM2* in Raji and
945 *Raji-CXCR5$^{oe}$* cells after 24 hours treatment with either Bleomycin (5µg/ml), Nutlin-3a (10µM),
946 or Bleomycin (5µg/ml) + Nutlin-3a (10µM). p= 0.0003 for Raji (DMSO) vs *Raji-CXCR5$^{oe}$* , p=

947 0.0176 for Raji (DMSO) vs *Raji-CXCR5$^{oe}$* and p<0.0001 Raji (DMSO) vs *Raji-CXCR5$^{oe}$* .

948 Tukey's multiple comparison test. Data are mean ± SEM for n=3 samples.

949

950 **Supplementary table 1. Primer sequences**

| Transcript name | Primer sequences for qPCR (5' to 3') |
|---|---|
| ACTB-FP | GATGATGATATCGCCGCGCT |
| ACTB-RP | GAATCCTTCTGACCCATGCC |
| CXCR5-FP | AGATTCTCTTCGCCAAAGTC |
| CXCR5-RP | CACCAGCATGGGCAGCAGGAAT |
| CXCL13-FP | GAAGTTCATCTCGACATCTC |
| CXCL13-RP | GAATTCGATCAATGAAGCGT |
| CCR7-FP | GTACTCCATCATTTGTTTCGTG |
| CCR7-RP | CAGAAGGGAAGGGTCAGGAG |
| CDKN1A-FP | CTGGAGACTCTCAGGGTCGAAA |
| CDKN1A-RP | GATTAGGGCTTCCTCTTGGAGAA |
| DDB2-FP | TCTACTCGCTGCCGCACAGG |
| DDB2-RP | TCGGGACTGAAACAAGCTGCGT |
| PTP4A1-FP | TAAGACAAAAGCGGCGTGGAGC |
| PTP4A1-RP | ACGCAGCCGCATTTTAGGACG |
| HAUSP-FP | CAGCCTGCTACAGACGTTAT |
| HAUSP-RP | CCCACCCAAATGACTTTGTTA |
| MDM2-FP | GAACTTGGTAGTAGTCAATCAGC |
| MDM2-RP | CTCTCCTTCTAGATGAGGTAG |
| PIRH2-FP | CCGCTTGTGTCATGATAACAA |
| PIRH2-RP | CCACAGTTTTCACAGTGATACTGC |
| ARF1-FP | CTTAAGCTGGGTGAGATCGTGAC |
| ARF1-RP | CTCTCTGTCATTGCTGTCCAC |
| ARFBP1-FP | CGGCTTTTCCTGAAGAAGGGAC |
| ARFBP1-RP | GTTTCCAAAGGCTTCAGAGCAGC |
| TP53-FP | ACTTTGCGTTCGGGCTGGGA |
| TP53-RP | GTCTGGCTGCCAATCCAGGGA |
| COP1-FP | GTCCCAAGTGTAACTATGTTG |
| COP1-RP | CTTGGTCAGTTCCCAACCAATC |
| MBD1-FP | CTGTCGAGCACAGAGAATTG |
| MBD1-FP | CGTTCACACTTGCAGAACAG |
| CTCF-FP | CCGTTACTGTGATGCTGTGT |
| CTCF-RP | GAAGGTCTTATCGCAGTGGC |
| | **Primers for shRNA-Knockdown (5' to 3')** |
| shRNA-MBD1 | CCGGGAACAGAGAATGTTTAA |
| shRNA-MYC#1 | CCTGAGACAGATCAGCAACAA |
| shRNA-MYC#2 | CAGTTGAAACACAAACTTGAA |
| shRNA-CTCF | ACGTGTCCACGGCGTTCAAAT |
| | ***CXCL13* guide RNA sequence for CRISPR/Cas9-knockout** |
| hCXCL13-gRNA1-FP | AGGTCTATTACACAAGCTTG |
| hCXCL13-gRNA2-RP | CAAGCTTGTGTAATAGACCT |
| hCXCL13-gRNA2-FP | GAACAAGTCAATTGTGTGTG |
| hCXCL13-gRNA2-RP | CACACACAATTGACTTGTTC |
| | **Primer sequences for ChIP analysis** |
| Primers | Primer sequence |
| CTCF-PP1_FP | CAAGCTCATGCGTGTGCAAG |
| CTCF-PP1_RP | CCTACCAGTCTTTTCCATCTC |
| CTCF-PP2_FP | GGAGTTGTTCTGAATAACCT |
| CTCF-PP2_RP | GCTTGTGTTGTGATAAGGGG |
| | **Primers for 3C assay** |
| CCNG2-int-PCR1-FP | GAGATCATGACTCTCACAGAC |

| | |
|---|---|
| CXCL13-int-PCR1-RP | GTTCTGATTTCAGGCATTGCC |
| CCNG2-nested-FP | ACGTAGATCTCTTTCGCTCCCTTGAATAAATG |
| CXCL13-nested-RP | GTCCTTCACCTTAAGGAGAG |

951
952 **Supplementary table 2 for antibodies for flow cytometry, western blotting, Immunoprecipitation**
953 **and ChIP assays**
954

| Antibody name | Purpose | Product/Manufacturer |
|---|---|---|
| CXCR5-APC | FACS | Biolegend (356907) |
| CXCR4-PE | FACS | Biolegend (306505) |
| CXCR3-BV421 | FACS | Biolegend (353715) |
| APC-Isotype control | FACS | Biolegend (400121) |
| PE-Isotype control | FACS | Biolegend (400111) |
| BV-421-Isotype control | FACS | Biolegend (400341) |
| BCL6 | WB | GeneTex#GTC101338 |
| β-actin | WB | Biolegend#643801 |
| Histone H3 | WB | Biolegend (819411) |
| γH2AX | ChIP | Abcam #ab20669 |
| CTCF | ChIP, WB | Active Motif #61932 |
| CXCR5 | WB | GeneTex#GTX100351 |
| p53 | WB | Biolegend# 645805 |
| MDM2 | WB | SANTACRUZ#sc-5304 |
| CXCL13 | WB, IP | AF801, R&D systems |
| MBD1 | WB | 39858, Active motif |
| RNAPII | ChIP | 61082, Active motif |

955
956
957
958
959
960
961
962
963
964

965 **References**


966 **1.** Cyster, J.G., et al., *Follicular stromal cells and lymphocyte homing to follicles.* Immunol
967 Rev, 2000. 176: p. 181-93.
968 2. Gunn, M.D., et al., *A B-cell-homing chemokine made in lymphoid follicles activates*
969 *Burkitt's lymphoma receptor-1.* Nature, 1998. 391(6669): p. 799-803.
970 3. Legler, D.F., et al., *B cell-attracting chemokine 1, a human CXC chemokine expressed in*
971 *lymphoid tissues, selectively attracts B lymphocytes via BLR1/CXCR5.* J Exp Med, 1998.
972 187(4): p. 655-60.
973 4. El-Haibi, C.P., et al., *Differential G protein subunit expression by prostate cancer cells*
974 *and their interaction with CXCR5.* Molecular Cancer, 2013. 12(1): p. 64.
975 5. Rao, D.A., et al., *Pathologically expanded peripheral T helper cell subset drives B cells*
976 *in rheumatoid arthritis.* Nature, 2017. 542(7639): p. 110-114.
977 6. Kobayashi, S., et al., *A distinct human CD4+ T cell subset that secretes CXCL13 in*
978 *rheumatoid synovium.* Arthritis Rheum, 2013. 65(12): p. 3063-72.
979 7. Yoshitomi, H., et al., *Human Sox4 facilitates the development of CXCL13-producing*
980 *helper T cells in inflammatory environments.* Nature Communications, 2018. 9(1): p.
981 3762.
982 8. Manzo, A., et al., *Mature antigen-experienced T helper cells synthesize and secrete the B*
983 *cell chemoattractant CXCL13 in the inflammatory environment of the rheumatoid joint.*
984 Arthritis Rheum, 2008. 58(11): p. 3377-87.
985 9. Förster, R., et al., *A putative chemokine receptor, BLR1, directs B cell migration to*
986 *defined lymphoid organs and specific anatomic compartments of the spleen.* Cell, 1996.
987 87(6): p. 1037-47.
988 10. Hussain, S.K., et al., *Serum levels of the chemokine CXCL13, genetic variation in*
989 *CXCL13 and its receptor CXCR5, and HIV-associated non-hodgkin B-cell lymphoma*
990 *risk.* Cancer Epidemiol Biomarkers Prev, 2013. 22(2): p. 295-307.
991 11. Bürkle, A., et al., *Overexpression of the CXCR5 chemokine receptor, and its ligand,*
992 *CXCL13 in B-cell chronic lymphocytic leukemia.* Blood, 2007. 110(9): p. 3316-25.
993 12. Kurtova, A.V., et al., *Mantle cell lymphoma cells express high levels of CXCR4, CXCR5,*
994 *and VLA-4 (CD49d): importance for interactions with the stromal microenvironment and*
995 *specific targeting.* Blood, 2009. 113(19): p. 4604-13.
996 13. Beider, K., et al., *CXCL13 chemokine is a novel player in multiple myeloma osteolytic*
997 *microenvironment, M2 macrophage polarization, and tumor progression.* Journal of
998 Hematology & Oncology, 2022. 15(1): p. 144.
999 14. Kazanietz, M.G., M. Durando, and M. Cooke, *CXCL13 and Its Receptor CXCR5 in*
1000 *Cancer: Inflammation, Immune Response, and Beyond.* Frontiers in Endocrinology, 2019.
1001 10(471).
1002 15. Singh, S., et al., *Clinical and biological significance of CXCR5 expressed by prostate*
1003 *cancer specimens and cell lines.* Int J Cancer, 2009. 125(10): p. 2288-95.
1004 16. Panse, J., et al., *Chemokine CXCL13 is overexpressed in the tumour tissue and in the*
1005 *peripheral blood of breast cancer patients.* British Journal of Cancer, 2008. 99(6): p.
1006 930-938.
1007 17. Ammirante, M., et al., *Tissue injury and hypoxia promote malignant progression of*
1008 *prostate cancer by inducing CXCL13 expression in tumor myofibroblasts.* Proc Natl Acad
1009 Sci U S A, 2014. 111(41): p. 14776-81.

1010 18. Zhu, Z., et al., *CXCL13-CXCR5 axis promotes the growth and invasion of colon cancer*
1011 *cells via PI3K/AKT pathway.* Mol Cell Biochem, 2015. 400(1-2): p. 287-95.
1012 19. Bugatti, S., et al., *High expression levels of the B cell chemoattractant CXCL13 in*
1013 *rheumatoid synovium are a marker of severe disease.* Rheumatology (Oxford), 2014.
1014 53(10): p. 1886-95.
1015 20. Shi, K., et al., *Lymphoid chemokine B cell-attracting chemokine-1 (CXCL13) is expressed*
1016 *in germinal center of ectopic lymphoid follicles within the synovium of chronic arthritis*
1017 *patients.* J Immunol, 2001. 166(1): p. 650-5.
1018 21. Krumbholz, M., et al., *Chemokines in multiple sclerosis: CXCL12 and CXCL13 up-*
1019 *regulation is differentially linked to CNS immune cell recruitment.* Brain, 2006. 129(Pt
1020 1): p. 200-11.
1021 22. Lee, H.T., et al., *Serum BLC/CXCL13 concentrations and renal expression of*
1022 *CXCL13/CXCR5 in patients with systemic lupus erythematosus and lupus nephritis.* J
1023 Rheumatol, 2010. 37(1): p. 45-52.
1024 23. Barone, F., et al., *Association of CXCL13 and CCL21 expression with the progressive*
1025 *organization of lymphoid-like structures in Sjögren's syndrome.* Arthritis Rheum, 2005.
1026 52(6): p. 1773-84.
1027 24. Meraouna, A., et al., *The chemokine CXCL13 is a key molecule in autoimmune*
1028 *myasthenia gravis.* Blood, 2006. 108(2): p. 432-40.
1029 25. Weiss, J.M., et al., *Novel CXCL13 transgenic mouse: inflammation drives pathogenic*
1030 *effect of CXCL13 in experimental myasthenia gravis.* Oncotarget, 2016. 7(7): p. 7550-62.
1031 26. Dai, S., et al., *Intratumoral CXCL13(+)CD8(+)T cell infiltration determines poor*
1032 *clinical outcomes and immunoevasive contexture in patients with clear cell renal cell*
1033 *carcinoma.* J Immunother Cancer, 2021. 9(2).
1034 27. Wang, G.Z., et al., *The chemokine CXCL13 in lung cancers associated with*
1035 *environmental polycyclic aromatic hydrocarbons pollution.* Elife, 2015. 4.
1036 28. Zhang, G., et al., *Mesenchymal stem cells from bone marrow regulate invasion and drug*
1037 *resistance of multiple myeloma cells by secreting chemokine CXCL13.* Bosn J Basic Med
1038 Sci, 2020. 20(2): p. 209-217.
1039 29. Zhang, G., et al., *CXCL-13 Regulates Resistance to 5-Fluorouracil in Colorectal Cancer.*
1040 Cancer Res Treat, 2020. 52(2): p. 622-633.
1041 30. Medina, D.J., et al., *Mesenchymal stromal cells protect mantle cell lymphoma cells from*
1042 *spontaneous and drug-induced apoptosis through secretion of B-cell activating factor*
1043 *and activation of the canonical and non-canonical nuclear factor κB pathways.*
1044 Haematologica, 2012. 97(8): p. 1255-63.
1045 31. Biswas, S., et al., *CXCL13-CXCR5 co-expression regulates epithelial to mesenchymal*
1046 *transition of breast cancer cells during lymph node metastasis.* Breast Cancer Res Treat,
1047 2014. 143(2): p. 265-76.
1048 32. Garg, R., et al., *Protein Kinase C Epsilon Cooperates with PTEN Loss for Prostate*
1049 *Tumorigenesis through the CXCL13-CXCR5 Pathway.* Cell Rep, 2017. 19(2): p. 375-388.
1050 33. van de Pavert, S.A., et al., *Chemokine CXCL13 is essential for lymph node initiation and*
1051 *is induced by retinoic acid and neuronal stimulation.* Nat Immunol, 2009. 10(11): p.
1052 1193-9.
1053 34. Kim, S., N.-K. Yu, and B.-K. Kaang, *CTCF as a multifunctional protein in genome*
1054 *regulation and gene expression.* Experimental & Molecular Medicine, 2015. 47(6): p.
1055 e166-e166.

1056 35. Lai, A.Y., et al., *DNA methylation prevents CTCF-mediated silencing of the oncogene*
1057 *BCL6 in B cell lymphomas.* Journal of Experimental Medicine, 2010. 207(9): p. 1939-
1058 1950.
1059 36. Zhang, X., et al., *Large DNA Methylation Nadirs Anchor Chromatin Loops Maintaining*
1060 *Hematopoietic Stem Cell Identity.* Mol Cell, 2020. 78(3): p. 506-521.e6.
1061 37. Tate, P.H. and A.P. Bird, *Effects of DNA methylation on DNA-binding proteins and gene*
1062 *expression.* Curr Opin Genet Dev, 1993. 3(2): p. 226-31.
1063 38. Fujita, N., et al., *Mechanism of transcriptional regulation by methyl-CpG binding protein*
1064 *MBD1.* Mol Cell Biol, 2000. 20(14): p. 5107-18.
1065 39. Gothwal, S.K., et al., *BRD2 promotes antibody class switch recombination by facilitating*
1066 *DNA repair in collaboration with NIPBL.* Nucleic Acids Res, 2024.
1067 40. Gao, J., et al., *Integrative analysis of complex cancer genomics and clinical profiles using*
1068 *the cBioPortal.* Sci Signal, 2013. 6(269): p. pl1.
1069 41. Cerami, E., et al., *The cBio cancer genomics portal: an open platform for exploring*
1070 *multidimensional cancer genomics data.* Cancer Discov, 2012. 2(5): p. 401-4.
1071 42. de Bruijn, I., et al., *Analysis and Visualization of Longitudinal Genomic and Clinical*
1072 *Data from the AACR Project GENIE Biopharma Collaborative in cBioPortal.* Cancer
1073 Res, 2023. 83(23): p. 3861-3867.
1074 43. Lakin, N.D. and S.P. Jackson, *Regulation of p53 in response to DNA damage.* Oncogene,
1075 1999. 18(53): p. 7644-55.
1076 44. Bertram, K., et al., *Inhibitors of Bcl-2 and Bruton's tyrosine kinase synergize to abrogate*
1077 *diffuse large B-cell lymphoma growth in vitro and in orthotopic xenotransplantation*
1078 *models.* Leukemia, 2022. 36(4): p. 1035-1047.
1079 45. Dan, H.C., et al., *Akt-dependent regulation of NF-{kappa}B is controlled by mTOR and*
1080 *Raptor in association with IKK.* Genes Dev, 2008. 22(11): p. 1490-500.
1081 46. Villa, R., et al., *The methyl-CpG binding protein MBD1 is required for PML-RARalpha*
1082 *function.* Proc Natl Acad Sci U S A, 2006. 103(5): p. 1400-5.
1083 47. Basso, K. and R. Dalla-Favera, *BCL6: master regulator of the germinal center reaction*
1084 *and key oncogene in B cell lymphomagenesis.* Adv Immunol, 2010. 105: p. 193-210.
1085 48. Fujita, N., et al., *Methyl-CpG binding domain 1 (MBD1) interacts with the Suv39h1-HP1*
1086 *heterochromatic complex for DNA methylation-based transcriptional repression.* J Biol
1087 Chem, 2003. 278(26): p. 24132-8.
1088 49. Xu, X., et al., *Parallel comparison of Illumina RNA-Seq and Affymetrix microarray*
1089 *platforms on transcriptomic profiles generated from 5-aza-deoxy-cytidine treated HT-29*
1090 *colon cancer cells and simulated datasets.* BMC Bioinformatics, 2013. 14 Suppl 9(Suppl
1091 9): p. S1.
1092 50. Liu, J., et al., *Epigenetic priming improves salvage chemotherapy in diffuse large B-cell*
1093 *lymphoma via endogenous retrovirus-induced cGAS-STING activation.* Clinical
1094 Epigenetics, 2023. 15(1): p. 75.
1095 51. Bender, C.M., M.M. Pao, and P.A. Jones, *Inhibition of DNA methylation by 5-aza-2'-*
1096 *deoxycytidine suppresses the growth of human tumor cell lines.* Cancer Res, 1998. 58(1):
1097 p. 95-101.
1098 52. Fan, L., et al., *CXCL13 is androgen-responsive and involved in androgen induced*
1099 *prostate cancer cell migration and invasion.* Oncotarget, 2017. 8(32): p. 53244-53261.
1100 53. Nanan, K.K., et al., *TET-Catalyzed 5-Carboxylcytosine Promotes CTCF Binding to*
1101 *Suboptimal Sequences Genome-wide.* iScience, 2019. 19: p. 326-339.

1102 54. Vilarrasa-Blasi, R., et al., *Dynamics of genome architecture and chromatin function*
1103 *during human B cell differentiation and neoplastic transformation.* Nature
1104 Communications, 2021. 12(1): p. 651.
1105 55. Schmitt, A.D., et al., *A Compendium of Chromatin Contact Maps Reveals Spatially*
1106 *Active Regions in the Human Genome.* Cell Rep, 2016. 17(8): p. 2042-2059.
1107 56. Liu, Y.J., et al., *Mechanism of antigen-driven selection in germinal centres.* Nature,
1108 1989. 342(6252): p. 929-31.
1109 57. Mitkin, N.A., et al., *p53-dependent expression of CXCR5 chemokine receptor in MCF-7*
1110 *breast cancer cells.* Scientific Reports, 2015. 5(1): p. 9330.
1111 58. Legler, D.F., E. Uetz-von Allmen, and M.A. Hauser, *CCR7: roles in cancer cell*
1112 *dissemination, migration and metastasis formation.* Int J Biochem Cell Biol, 2014. 54: p.
1113 78-82.
1114 59. Leng, R.P., et al., *Pirh2, a p53-induced ubiquitin-protein ligase, promotes p53*
1115 *degradation.* Cell, 2003. 112(6): p. 779-91.
1116 60. Kubbutat, M.H., S.N. Jones, and K.H. Vousden, *Regulation of p53 stability by Mdm2.*
1117 Nature, 1997. 387(6630): p. 299-303.
1118 61. Chen, D., et al., *ARF-BP1/Mule is a critical mediator of the ARF tumor suppressor.* Cell,
1119 2005. 121(7): p. 1071-83.
1120 62. Rasmussen, K.D. and K. Helin, *Role of TET enzymes in DNA methylation, development,*
1121 *and cancer.* Genes Dev, 2016. 30(7): p. 733-50.
1122 63. Larsen, F., et al., *CpG islands as gene markers in the human genome.* Genomics, 1992.
1123 13(4): p. 1095-107.
1124 64. Singh, D.K., et al., *5-Azacytidine- and retinoic-acid-induced reprogramming of DCCs*
1125 *into dormancy suppresses metastasis via restored TGF-β-SMAD4 signaling.* Cell Rep,
1126 2023. 42(6): p. 112560.
1127 65. Tian, H., et al., *Tet-mediated DNA methylation dynamics affect chromosome*
1128 *organization.* Nucleic Acids Research, 2024.
1129 66. Nanavaty, V., et al., *DNA Methylation Regulates Alternative Polyadenylation via CTCF*
1130 *and the Cohesin Complex.* Mol Cell, 2020. 78(4): p. 752-764.e6.
1131 67. Jiang, D., et al., *TET3-mediated DNA oxidation promotes ATR-dependent DNA damage*
1132 *response.* EMBO reports, 2017. 18(5): p. 781-796-796.
1133 68. Chiecchio, L., et al., *Frequent upregulation of MYC in plasma cell leukemia.* Genes
1134 Chromosomes Cancer, 2009. 48(7): p. 624-36.
1135 69. Avet-Loiseau, H., et al., *Rearrangements of the c-myc oncogene are present in 15% of*
1136 *primary human multiple myeloma tumors.* Blood, 2001. 98(10): p. 3082-6.
1137 70. Zeidler, R., et al., *Breakpoints of Burkitt's lymphoma t(8;22) translocations map within a*
1138 *distance of 300 kb downstream of MYC.* Genes Chromosomes Cancer, 1994. 9(4): p. 282-
1139 7.
1140 71. Dominguez-Sola, D., et al., *The proto-oncogene MYC is required for selection in the*
1141 *germinal center and cyclic reentry.* Nat Immunol, 2012. 13(11): p. 1083-91.
1142 72. Huang, C., et al., *Cooperative transcriptional repression by BCL6 and BACH2 in*
1143 *germinal center B-cell differentiation.* Blood, 2014. 123(7): p. 1012-20.

# Paper outline

- CXCL13 expression in hematological, solid cancers
- CXCL13 regulation by DNA-methylation, MBD1, SE-CXCL13-TSS interaction
- Effect of CXCR5-CXCL13 axis on p53 target genes

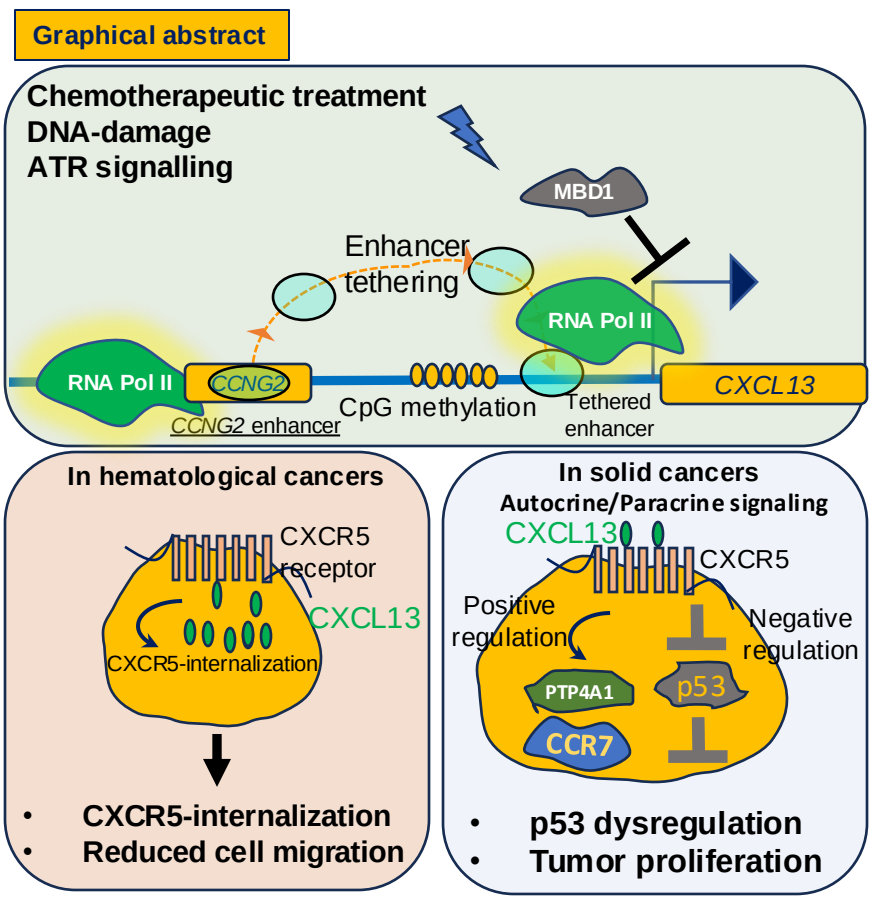


**Highlights:**

- **Aberrant *CXCL13* expression in hematological and solid cancers**
- **Chemotherapeutic treatment of cancer cells promotes *CXCL13* and *CXCR5* expression**
- **Distal super-enhancer on *CCNG2* interacts with *CXCL13* promoter**
- **CXCL13 expression in B-lymphomas prevents CXCR5-dependent migration**
- **CXCR5-CXCL13 axis encounters p53 function in hematological and solid cancer cells**

# Figure- 1 Aberrant CXCL13 expression hematological and solid cancers

**A. *CXCL13*: copy number values in *CXCL13* altered groups**

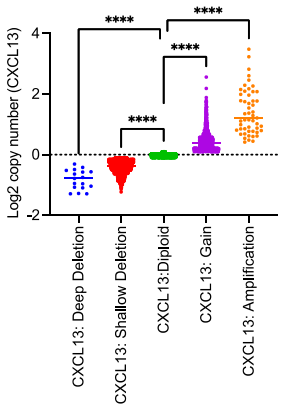


**B. *CXCL13* mRNA expression in different cancer types**

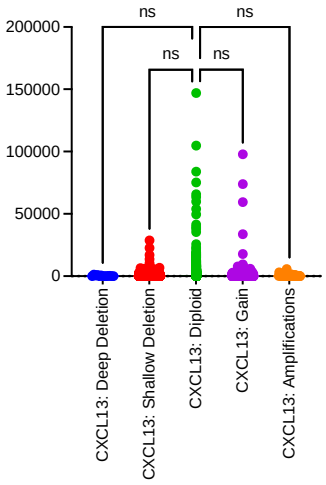


**C. *CXCR5* mRNA normalized to illumina Hiseq_RNAseqV2 in diploid cancers**

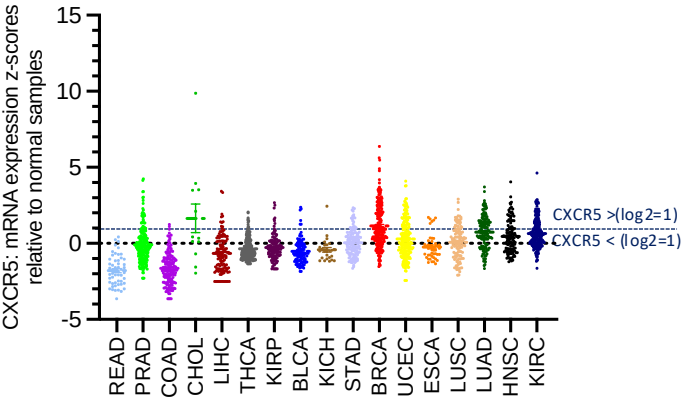


**D. *CXCL13* mRNA normalized to illumina Hiseq_RNAseqV2 in diploid cancer only**

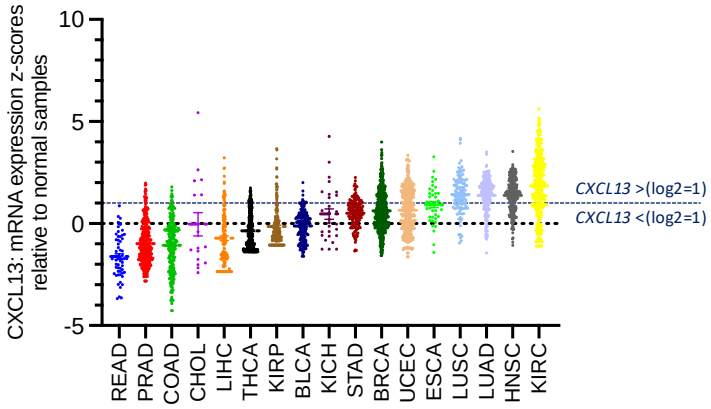


**E. Schematic of CXCR5 and CXCL13 overexpressing cancer cells activating autocrine/paracrine signaling and metastasis**

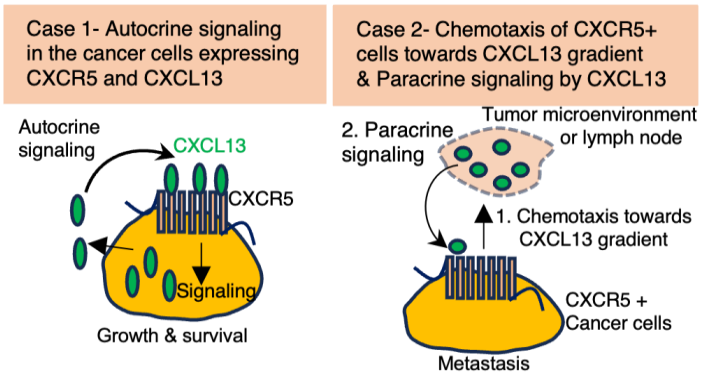


**F. *CXCL13* mRNA levels in B-lymphomas**

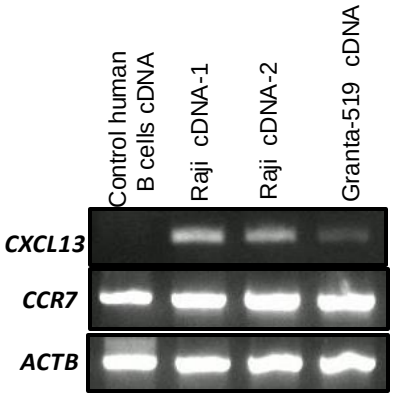


**G. Relative *CXCL13* transcript level in cancer cells**

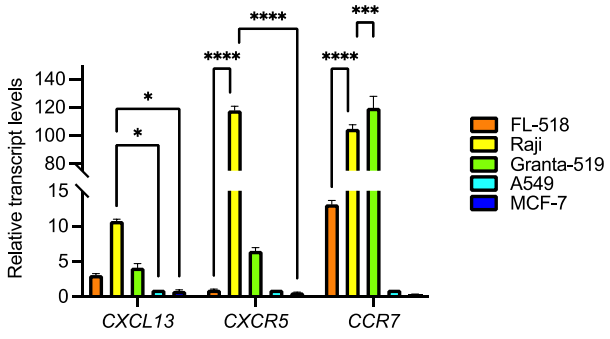


**H. CXCL13 expresion in solid cancers clls**

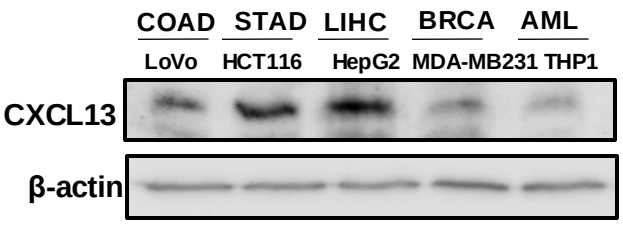

# Figure 2- DNA damage and Replication stress induce CXCL13 expression in cancer cells

**A. CXCL13 expression is induced by DNA-replication stress and DNA damage**

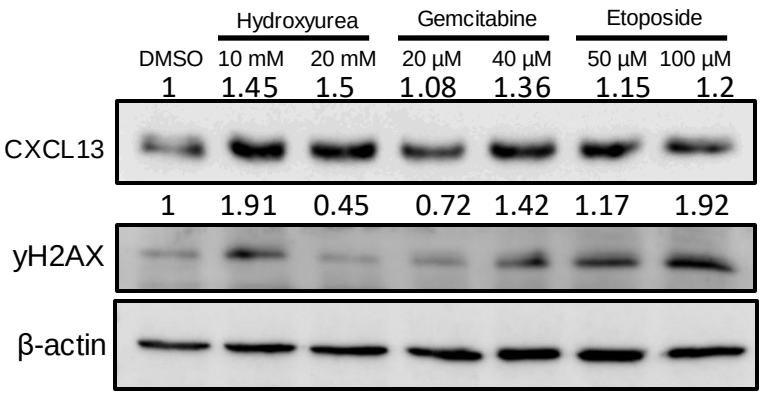


**B. Corelation between CXCL13 and γH2AX levels**

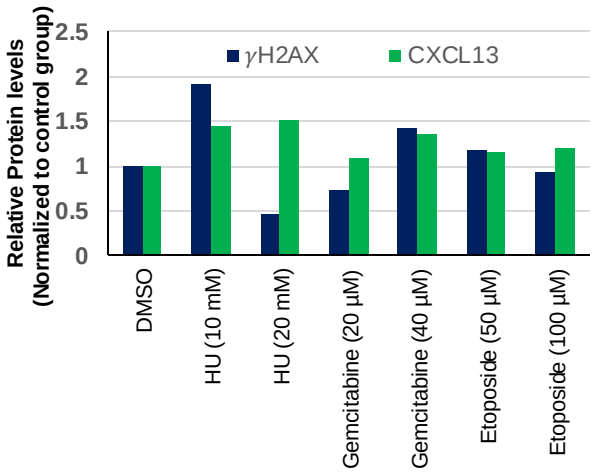


**C. Bleomycin and Nutlin-3a treatment increases CXCL13 levels**

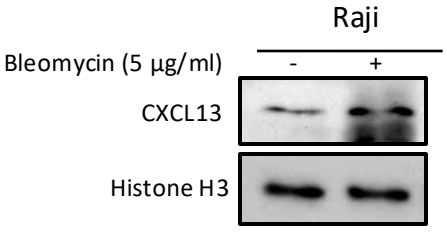


**D. Bleomycin and Nutlin-3a treatment induce *CXCL13* and *CXCR5* transcription**

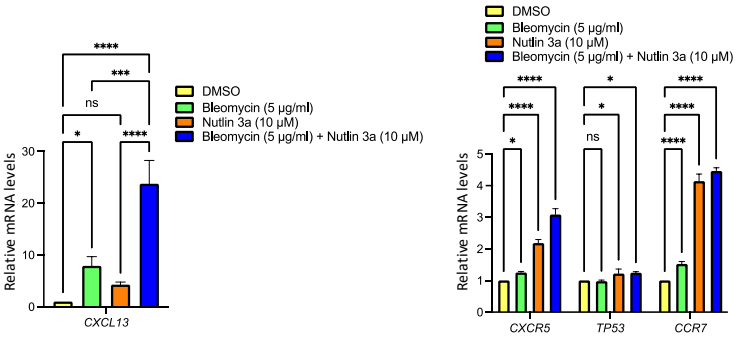


**E. Bleomycin and Nutlin-3a treatment increase surface CXCR5 expression**

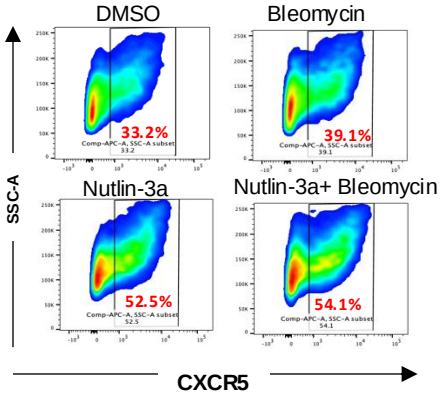


**F. BTK inhibitor Ibrutinib treatment induces the CXCL13 expression**

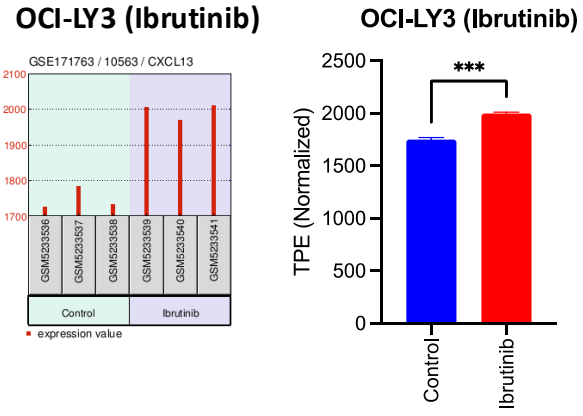


**G. CDK9 inhibitor induces the *CXCL13* expression**

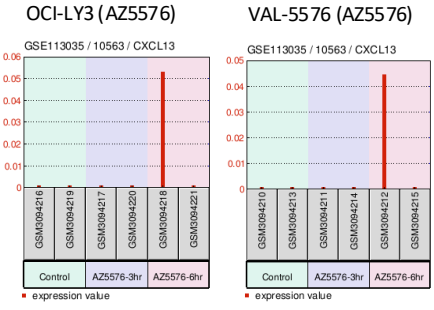


**H. ATR inhibition prominently reduces the CXCL13 expression**

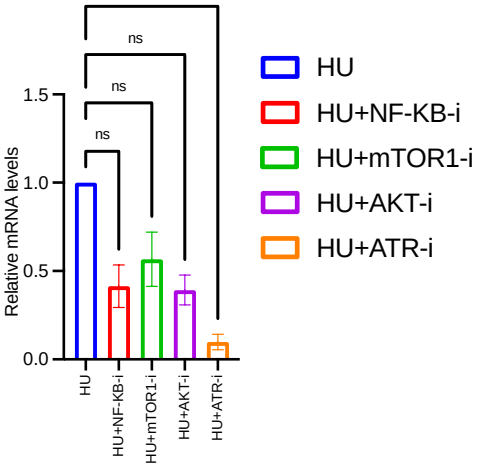

# Figure 3- MBD1 suppresses CXCL13 expresion in B-lymphoma cells

**A. RARA binding sites on the human *CXCL13* promoter**

**B. CTCF binding sites on the human *CXCL13* promoter**

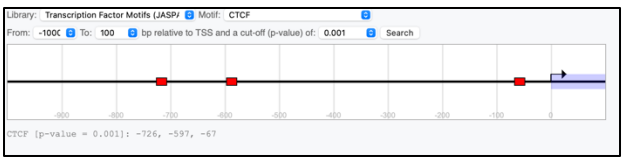


**C. p53 binding sites on the human *CXCL13* promoter**

**D. MYC binding sites on the human *CXCL13* promoter**

**E. MBD1 suppreses *CXCL13 expresion***

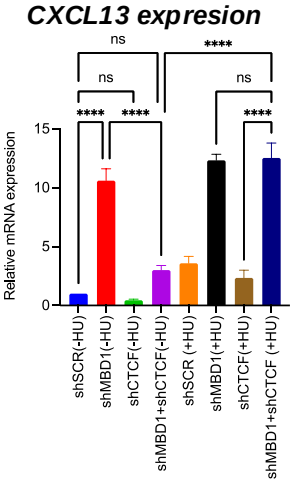


**F. Knockdown efficiency of MBD1 and CTCF in Raji cells**

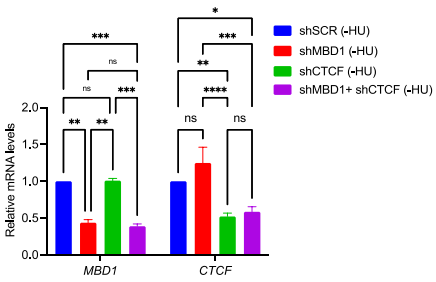


**G. MBD1 suppresses CXCL13 in HU depndent manner**

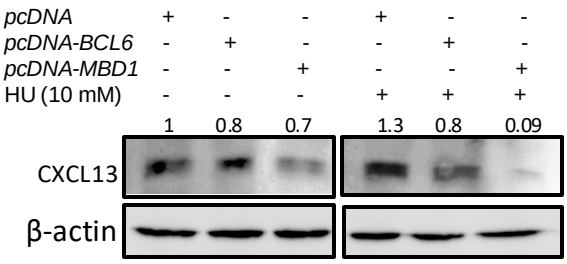


**H. HT29-cells treated with 5-Aza induces the *CXCL13* expression (GSE41586)**

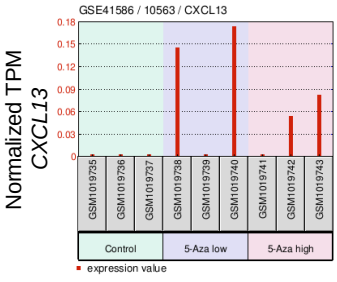


**I. 5-Aza treatment of OCI-LY3 cells induce *CXCL13*/*CXCR5* expression**

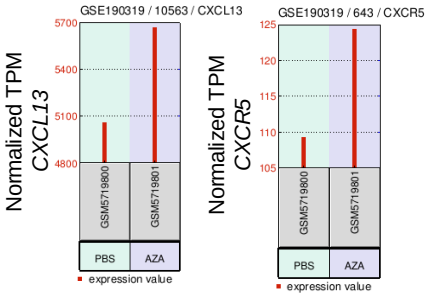


**J. MYC promotes CXCL13 expresion in the Raji cells**

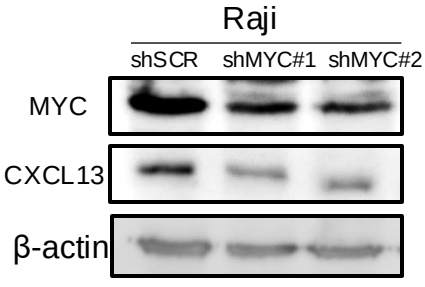

# Figure 4- Altered CTCF binding is associated with RNA-PolII enrichment at CXCL13 promoter

**A. CTCF binding on *CXCL13* locus IN 114 cell lines**

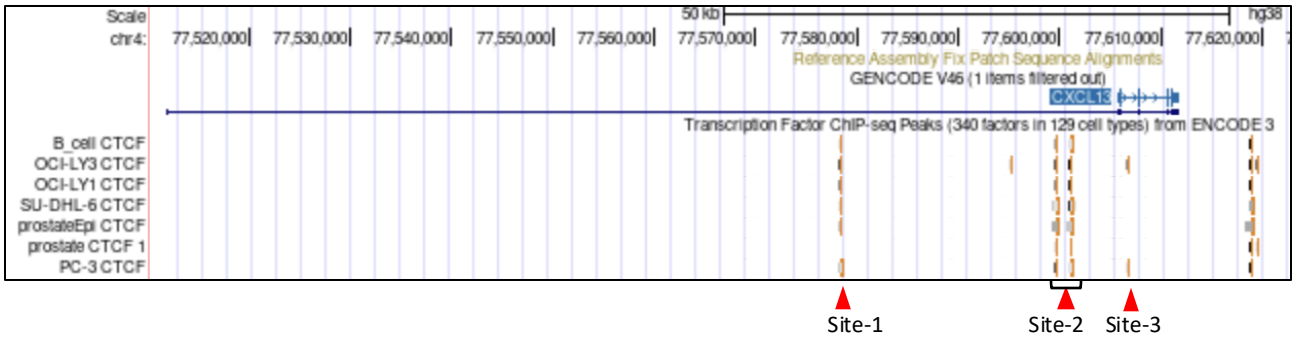


**B. Quantification of CTCF binding on Site-1, Site-2, Site-3 of *CXCL13* locus in 114 cell types**

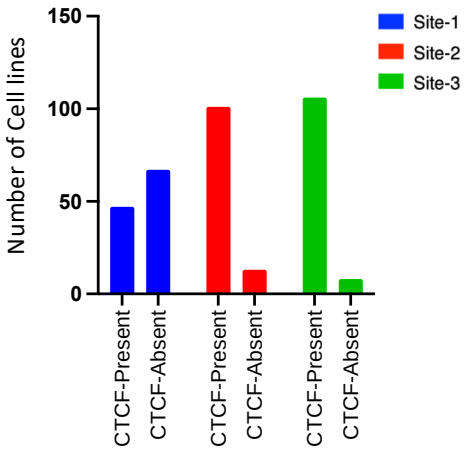


**C. CTCF binds to *CXCL13* promoter upon HU-treatment**

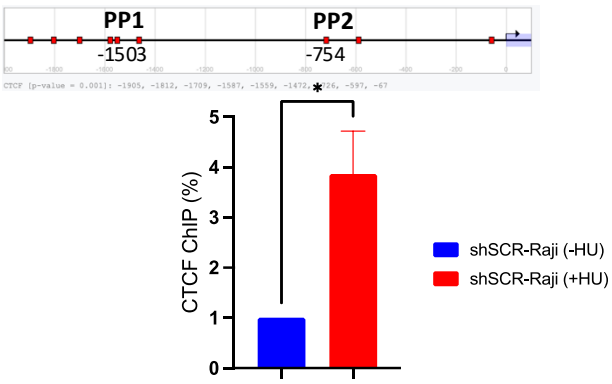


**D. Increased RNA-PolII binding at PP2 site upon HU-treatment**

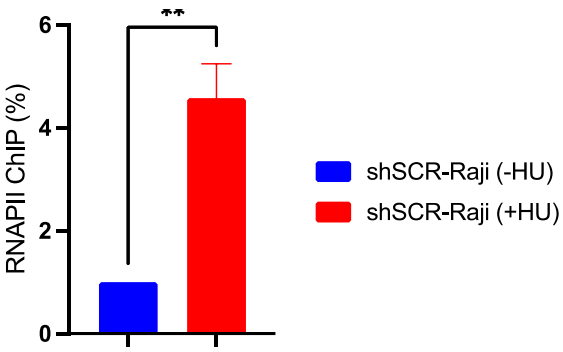


**E. Treatment of Bobocat339 (TET inhibitor) reduced the *CXCL13* expresion in HCT116**

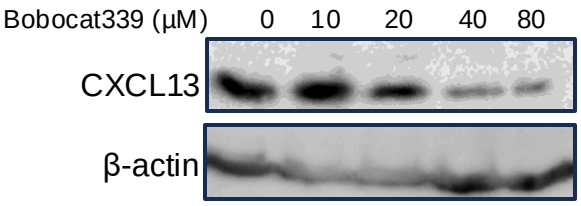

# Figure 5 Promoter conformational changes drive *CXCL13* expression in GCDBLs

## A. *CCNG2* enhancer interaction with *CXCL13* locus

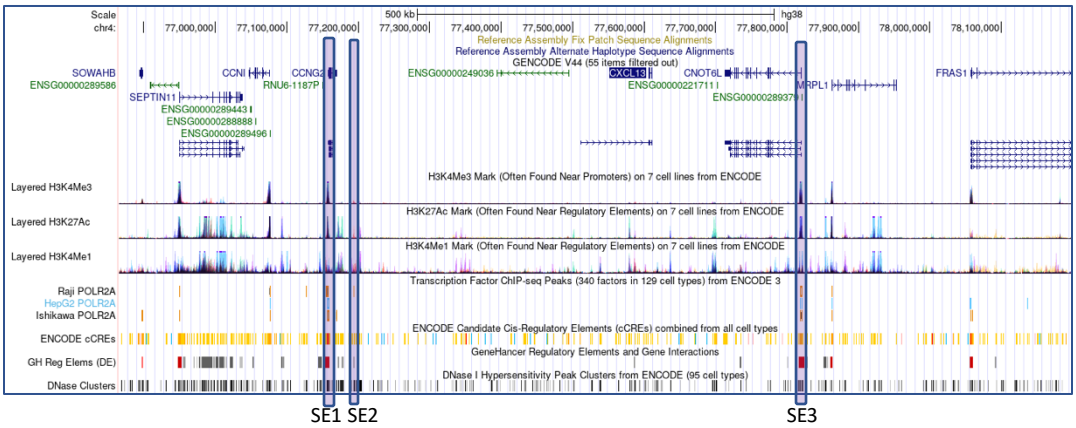


## B. HiC interaction in Mantle cell lymphoma and normal B cells surrounding *CXCL13*

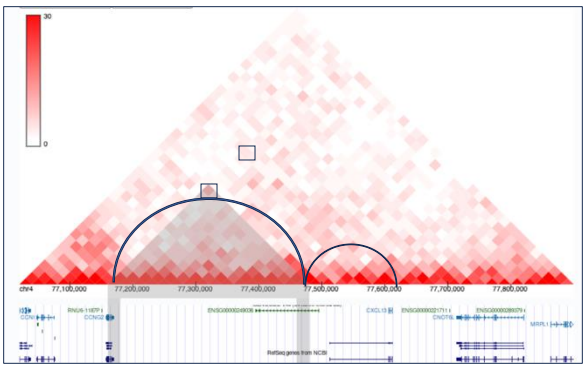

## C. Virtual 4C data constructed from Hi-C data of Spleen

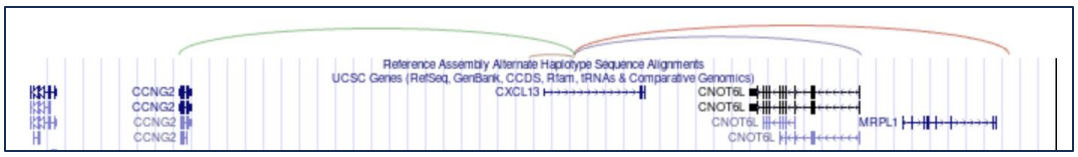

## D. Schematic of superenhancer identification and 3C asay for the *CXCL13*-TSS1

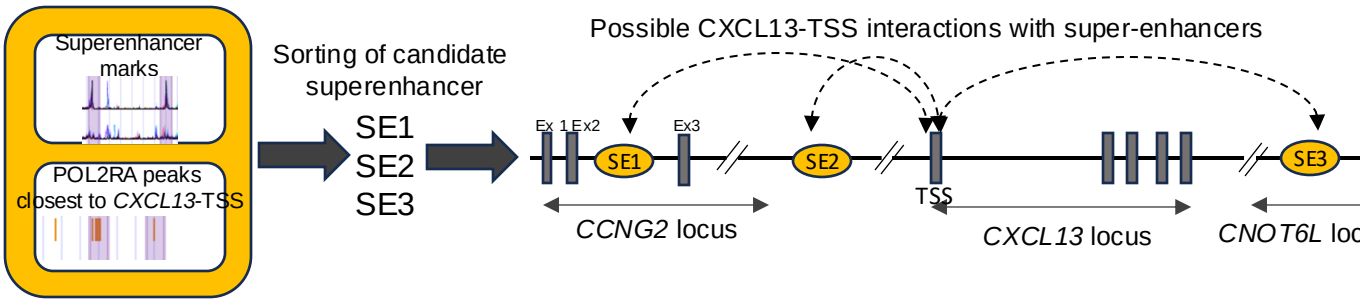


## E. Scheme of 3C asay based first and nested PCR

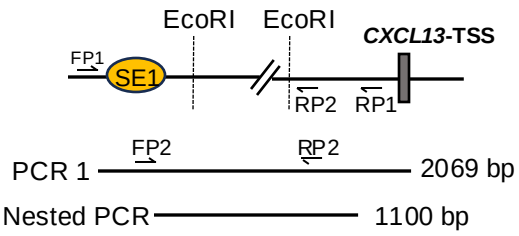


## F. Distal super-enhancer of *CCNG2* locus interacts with *CXCL13* TSS1

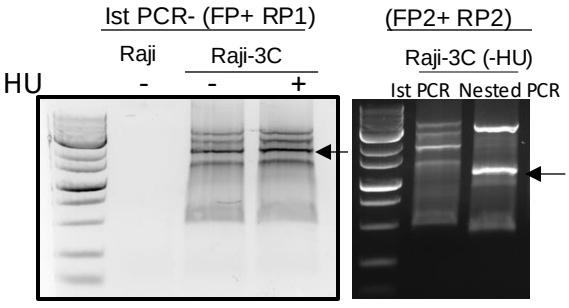


## G. SE1 and SE3 are evolutionary conserved among species

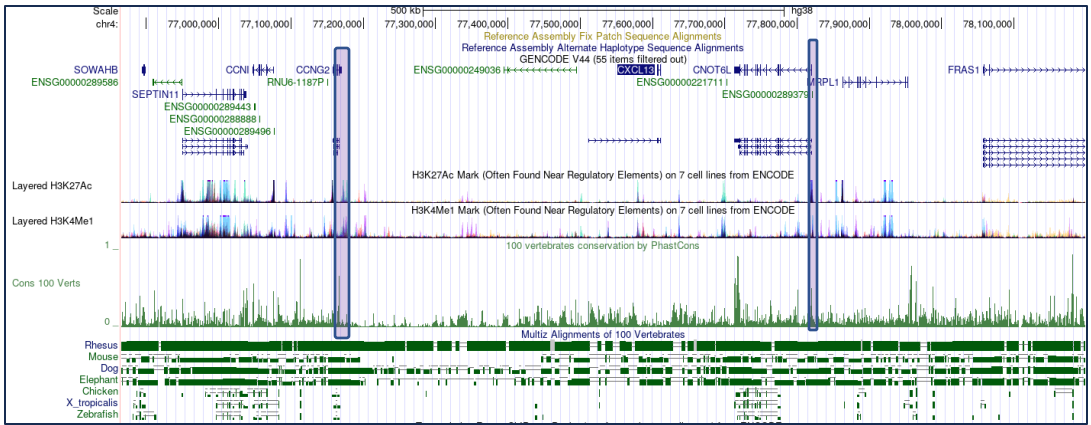

# Figure- 6 Induced CXCL13 expression in GCDBLs deprives Light Zone migration

**A. Migration of multiple B-lymphoma towards external CXCL13**

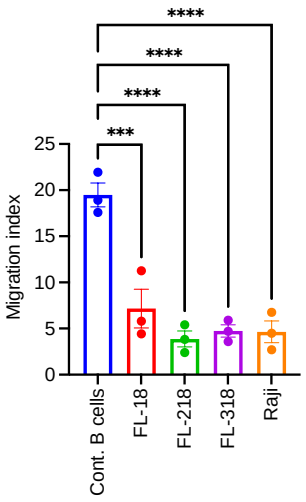


**B higher migration of Raij towards CXCL12 (DZ chemokine)**

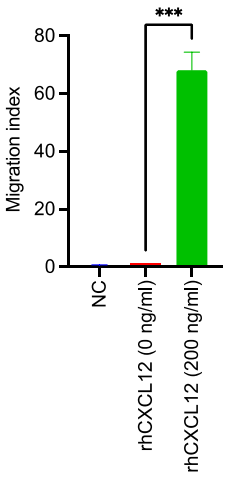


**C. Higher migration index of Raji cells towards CXCL12 than CXCL13**

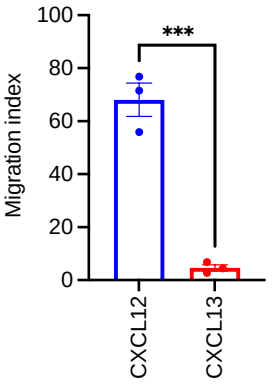


**D. CXCL13-Raji cells exhibits enhanced migration**

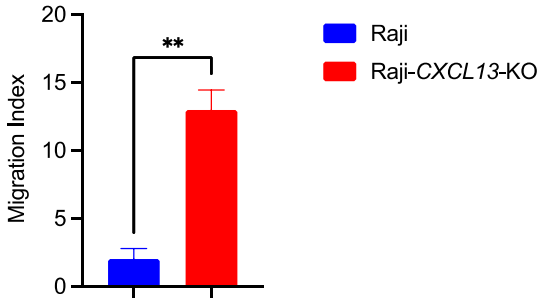


**E. CXCL13 IP in Raji**

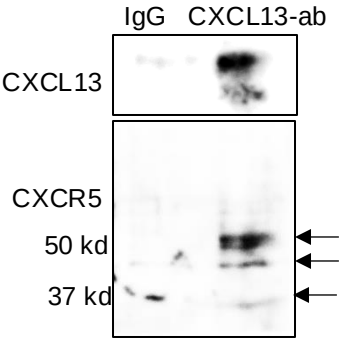


**F. Intracellular CXCR5 in Raji cells**

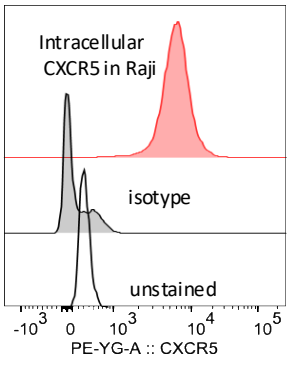


**G. CXCR5 receptor is drastically internalized in GCDBLs**

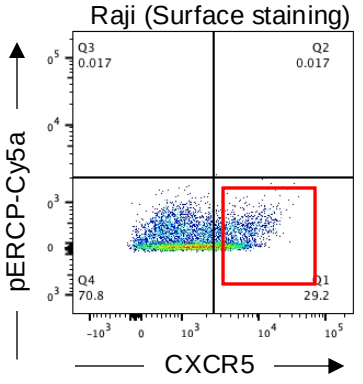

## Figure 7. CXCR5-CXCL13 axis promotes cell cycle progression and counteracts the p53 stablity

### A. Schematic of cell synchronization and proliferation assay

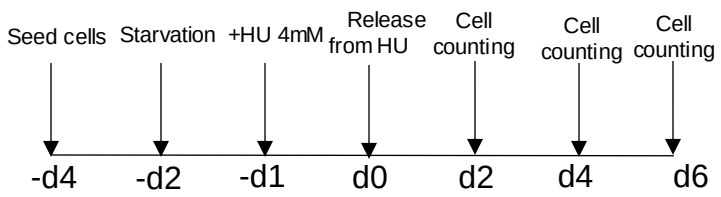


### B. Higher cellular proliferation in *Raji-CXCR5$^{oe}$* cells

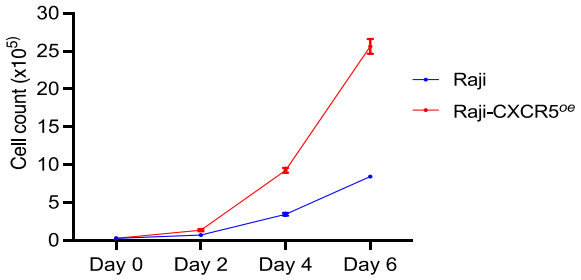


### C. CXCR5-CXCL13 axis promotes *CCR7* expression

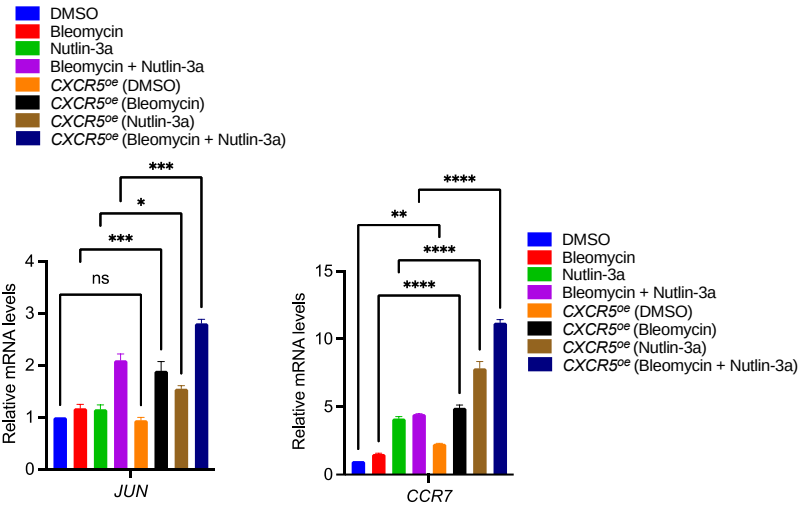


### D. CXCR5-CXCL13 axis reduced *TP53*

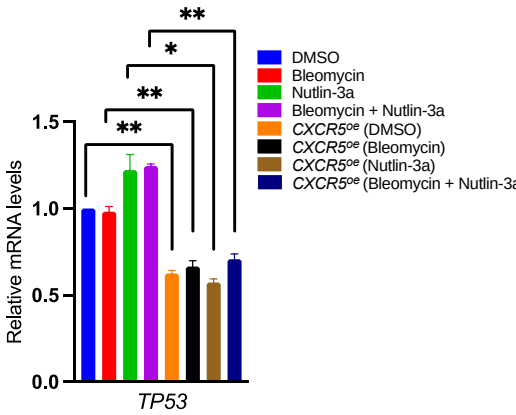


### E. CXCR5-CXCL13 axis counteracts p53 target genes

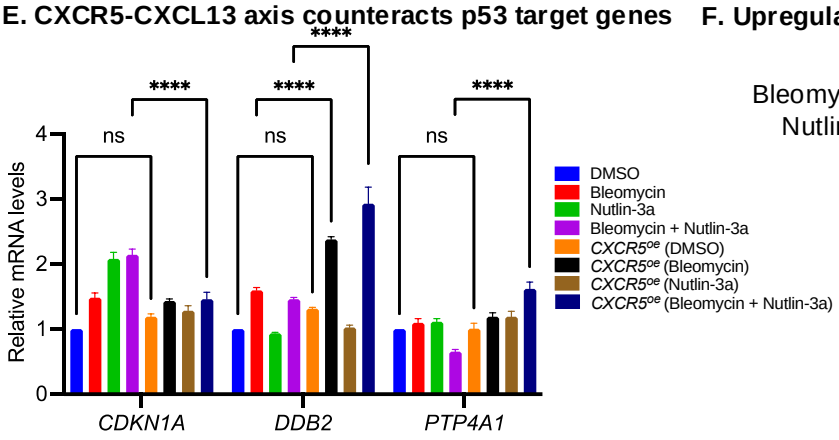


### F. Upregulation of PTP4A1 upon DNA damage in Raji cells

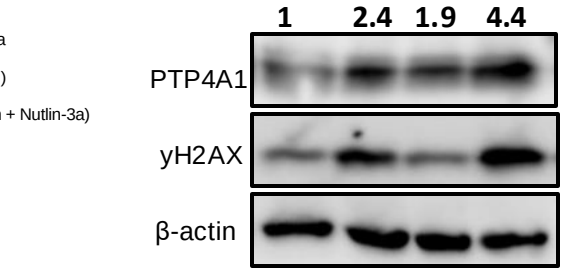


### G. Schematic of p53 degradation by ubiquitin ligases

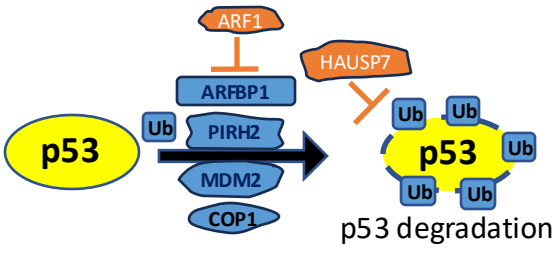


### H. Upregulation of *PIRH2*, *COP1* and downregulation of *HAUSP* mRNA in in *Raji-CXCR5$^{oe}$*

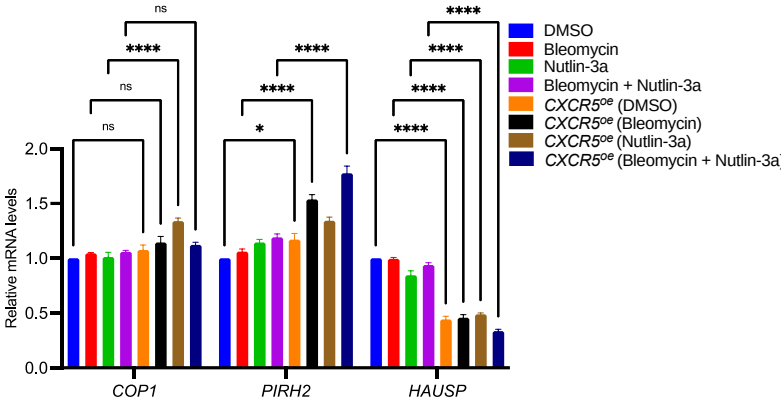


### I. CXCR5-CXCL13 axis affects p53 target genes in HCT116

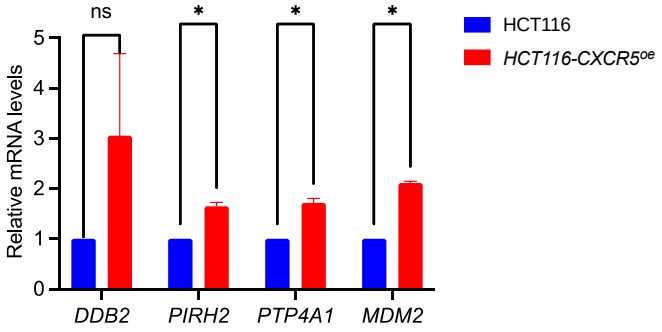


### J. CXCR5-CXCL13 axis promotes *PIRH2* in the HepG2 cells

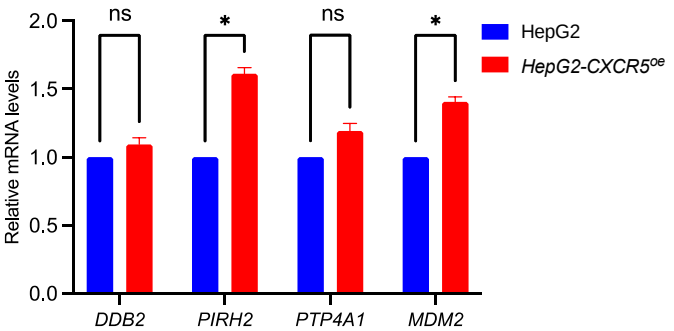

## Supplementary Figure 1

**A.**

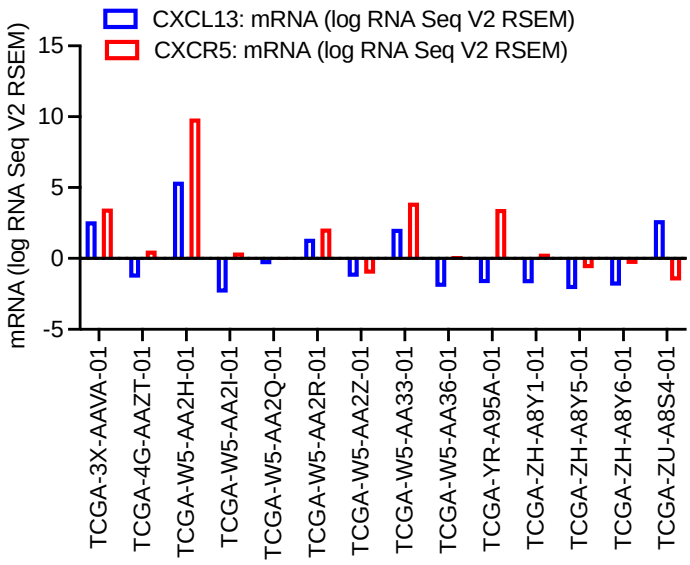


**B. UVM survival curver**

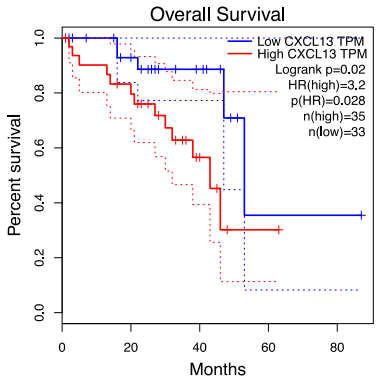


**C. GBM survival curve**

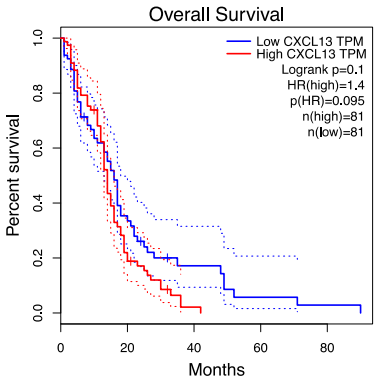


**D. AML survival curve**

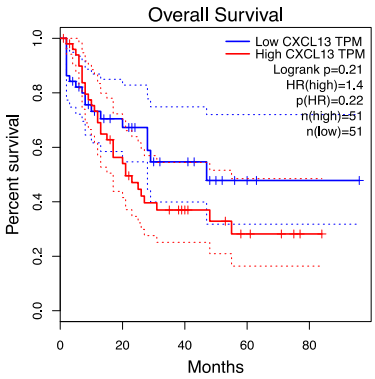


**E. Full blots to detect CXCL13 (12% PAGE, 20 min transfer)**

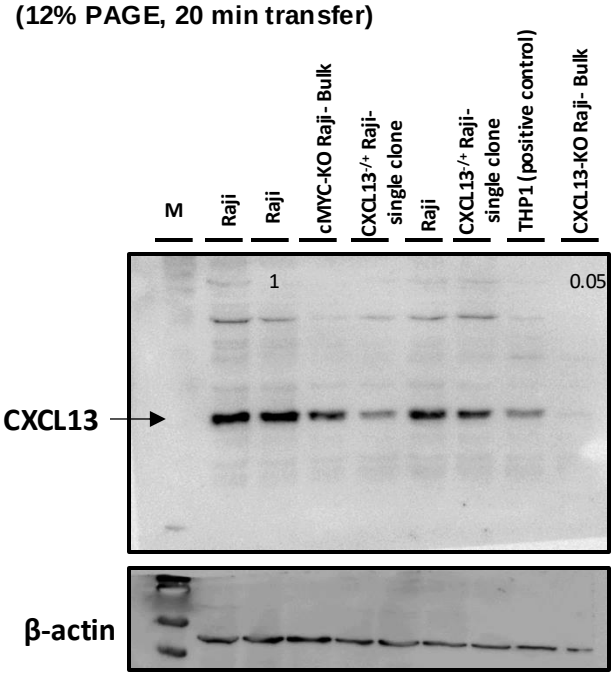

## Supplemetary Figure 2 Nutlin-3a treatment can activate mutant p53 in Raji cells

A. Bobocat-339 treatment reduces the CXCL13 expression in HCT116 cells

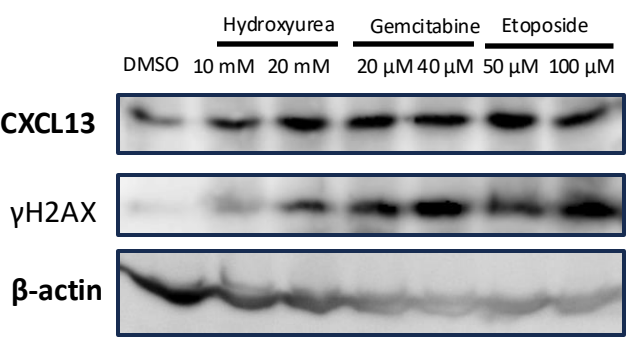


B. Nutlin-3a treatment of Raji cells

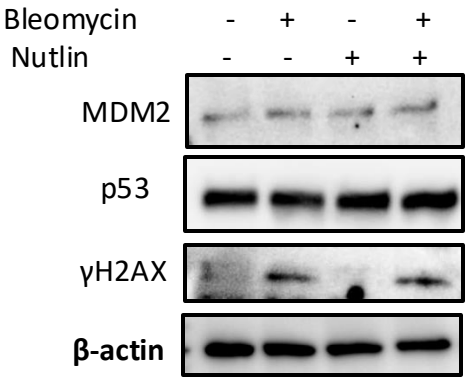


C. Nutlin-3a treatment can activate the mt-p53

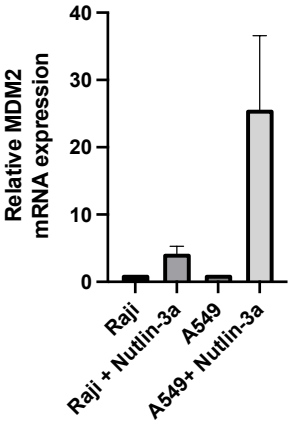


## Supplementary figure 3 - CTCF, RARA, and Myc binding sites are evolutionalry conserved on mouse CXCL13 pro

### A. RARA-binding sites on the mouse *Cxcl13* locus

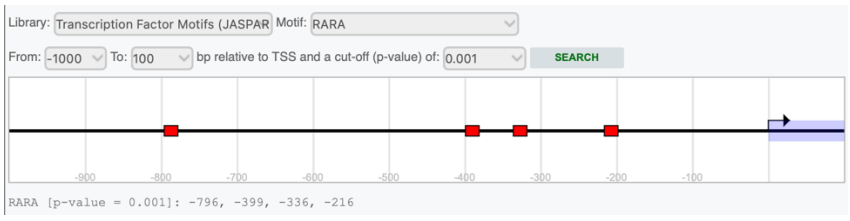


### B. CTCF binding sites on the mouse *Cxcl13* locus

### C. Myc binding sites on the mouse *Cxcl13* locus

**D.**

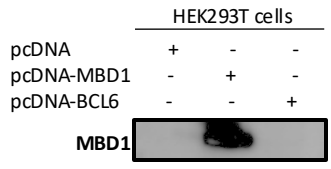


**E.**

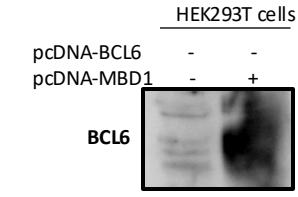

## Supplementary Figure 4

### A. Genetic location of human *CXCL13* locus and exon-intron distribution

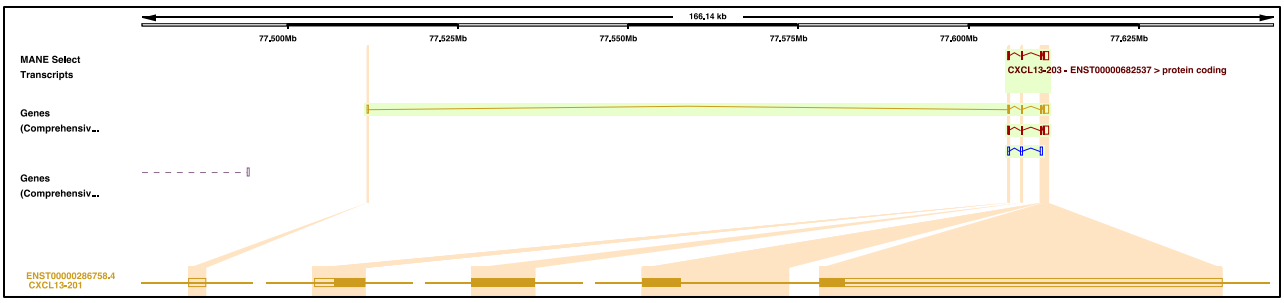


### B. CTCF binding on *CXCL13* locus IN 114 cell lines

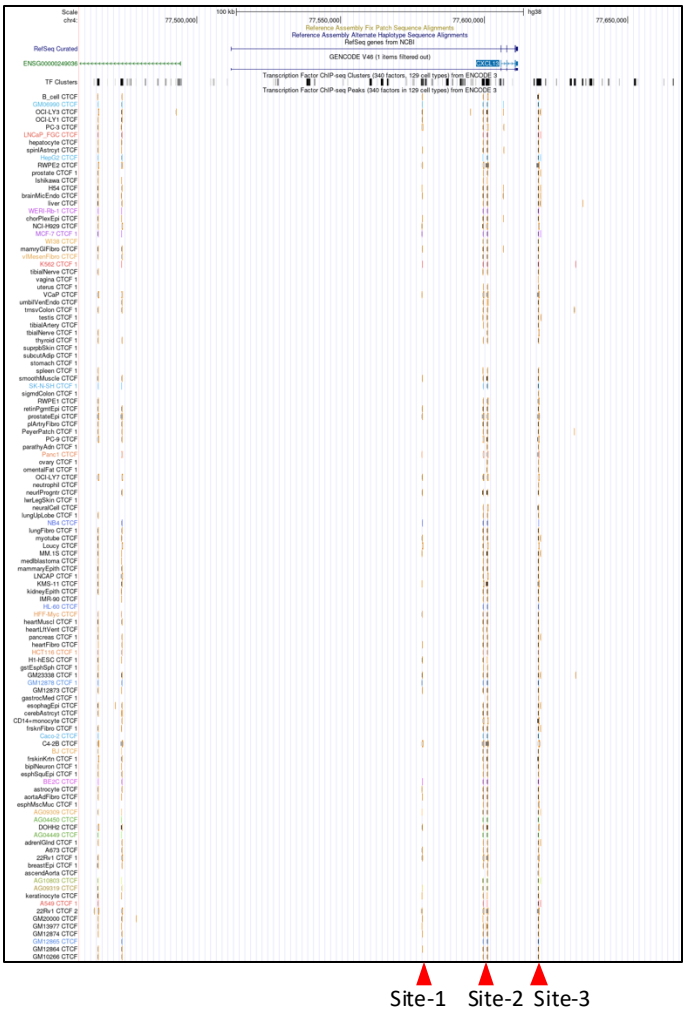


## Supplementary Figure 5- PBMC do not express the *CXCL13*

### A. Human PBMC does not express *CXCL13*

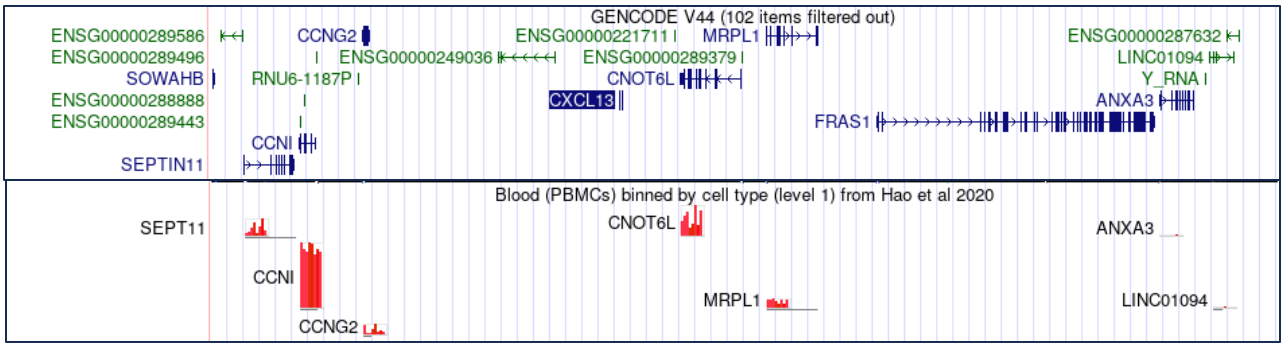


## Supplementary figure 6

### A. CXCR5 receptor is not mutated in the Raji cells.

```
Query                  1    MNYPLTLEMDLENLEDLFWELDRLDNYNDTSLVENHLCPATEGPLMASFKAVFVPVAYSL    60
                            MNYPLTLEMDLENLEDLFWELDRLDNYNDTSLVENHLCPATEGPLMASFKAVFVPVAYSL
P32302 CXCR5_HUMAN     1    MNYPLTLEMDLENLEDLFWELDRLDNYNDTSLVENHLCPATEGPLMASFKAVFVPVAYSL    60

Query                 61    IFLLGVIGNVLVLVILERHRQTRSSTETFLFHLAVADLLLVFILPFAVAEGSVGWVLGTF   120
                            IFLLGVIGNVLVLVILERHRQTRSSTETFLFHLAVADLLLVFILPFAVAEGSVGWVLGTF
P32302 CXCR5_HUMAN    61    IFLLGVIGNVLVLVILERHRQTRSSTETFLFHLAVADLLLVFILPFAVAEGSVGWVLGTF   120

Query                121    LCKTVIALHKVNFYCSSLLLACIAVDRYLAIVHAVHAYRHRRLLSIHITCGTIWLVGFLL   180
                            LCKTVIALHKVNFYCSSLLLACIAVDRYLAIVHAVHAYRHRRLLSIHITCGTIWLVGFLL
P32302 CXCR5_HUMAN   121    LCKTVIALHKVNFYCSSLLLACIAVDRYLAIVHAVHAYRHRRLLSIHITCGTIWLVGFLL   180

Query                181    ALPEILFAKVSQGHHNNSLPRCTFSQENQAETHAWFTSRFLYHVAGFLLPMLVMGWCYVG   240
                            ALPEILFAKVSQGHHNNSLPRCTFSQENQAETHAWFTSRFLYHVAGFLLPMLVMGWCYVG
P32302 CXCR5_HUMAN   181    ALPEILFAKVSQGHHNNSLPRCTFSQENQAETHAWFTSRFLYHVAGFLLPMLVMGWCYVG   240

Query                241    VVHRLRQAQRRPQRQKAVRVAILVTSIFFLCWSPYHIVIFLDTLARLKAVDNTCKLNGSL   300
                            VVHRLRQAQRRPQRQKAVRVAILVTSIFFLCWSPYHIVIFLDTLARLKAVDNTCKLNGSL
P32302 CXCR5_HUMAN   241    VVHRLRQAQRRPQRQKAVRVAILVTSIFFLCWSPYHIVIFLDTLARLKAVDNTCKLNGSL   300

Query                301    PVAITMCEFLGLAHCCLNPMLYTFAGVKFRSDLSRLLTKLGCTGPASLCQLFPSWRRSSL   360
                            PVAITMCEFLGLAHCCLNPMLYTFAGVKFRSDLSRLLTKLGCTGPASLCQLFPSWRRSSL
P32302 CXCR5_HUMAN   301    PVAITMCEFLGLAHCCLNPMLYTFAGVKFRSDLSRLLTKLGCTGPASLCQLFPSWRRSSL   360

Query                361    SESENATSLTTF                                                   372
                            SESENATSLTTF
P32302 CXCR5_HUMAN   361    SESENATSLTTF                                                   372
```

**Supplementary figure-7 CXCR5 overexpression induces the CXCL13 expression via a positive feedback**

**A. Higher CXCR5 levels in *Raji-CXCR5$^{oe}$* cells**

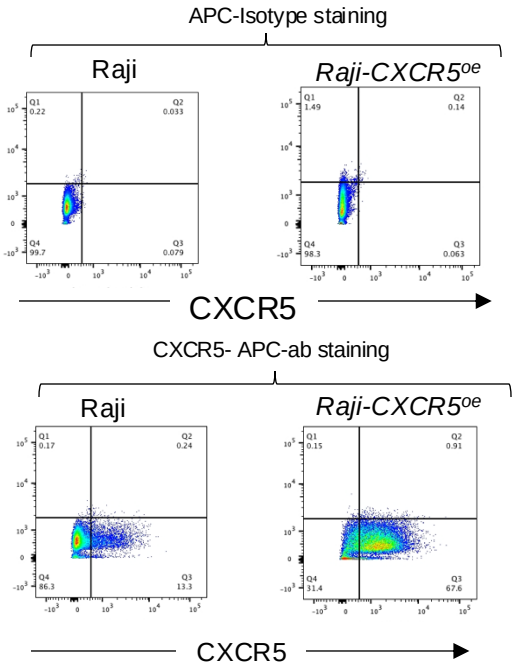


**B. Higher *CXCR5* mRNA levels in *Raji-CXCR5$^{oe}$* cells**

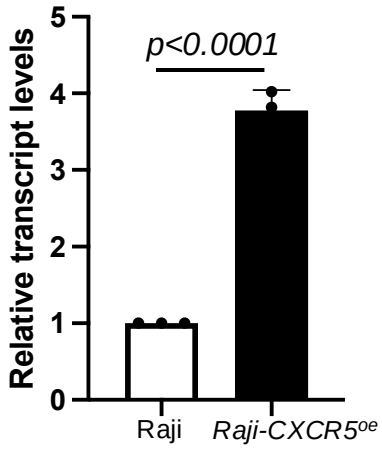


**C. Higher *CXCL13* mRNA levels in *Raji-CXCR5$^{oe}$* cells**

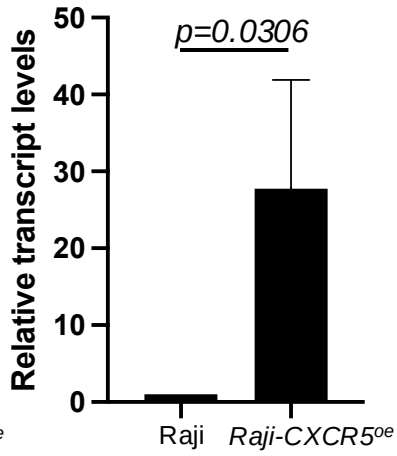


**D. CXCR5 overexpression does not induce the CXCL13 migration in Raji cells**

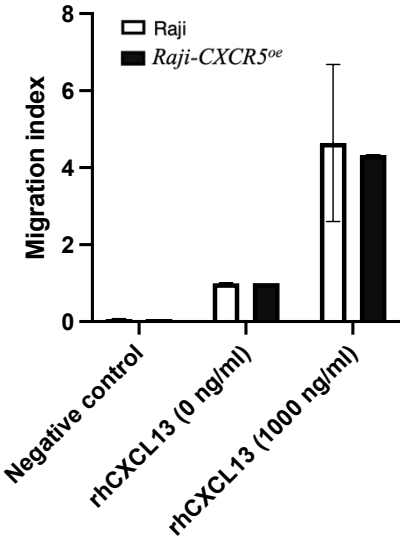

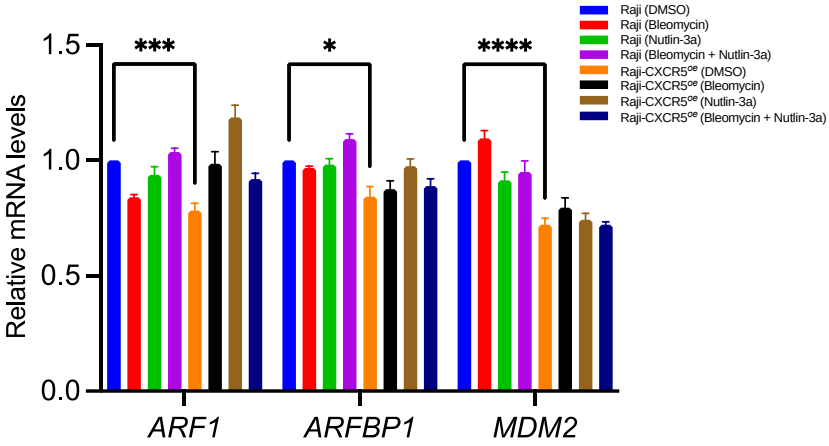
**E. *ARF1*, *ARFBP1*, and *MDM2* mRNA levels in *Raji-CXCR5$^{oe}$* cells**